Solar Wind Charge Exchange Contributions to the Diffuse X-ray Background

T. E. Cravens (with I. P. Robertson, S. L. Snowden, M. R. Collier, K. Kuntz, and M. Medvedev)

At the Local Bubble Bubble and Beyond II

Philadelphia, April 2008

Yohkoh X-Ray Image of the Solar Corona

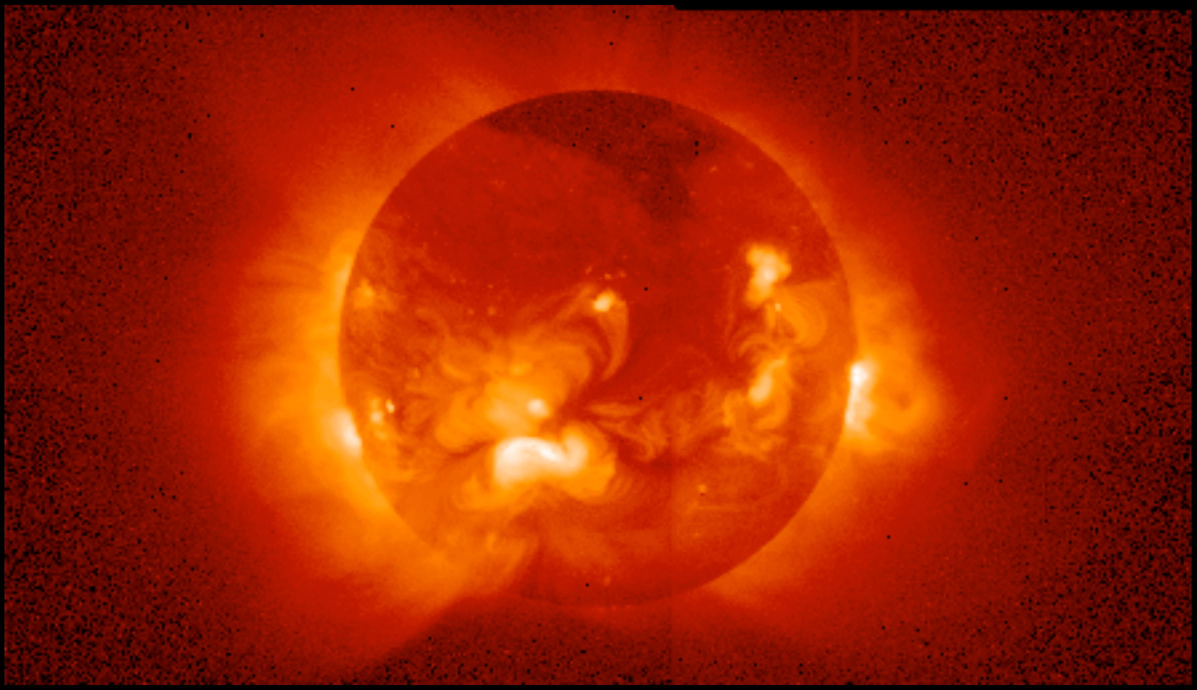

Other solar system x-ray sources: Earth (aurora and geocorona), Venus and Mars (disk and halo), comets, Jupiter (aurora and disk), Saturn (disk), heliosphere,……

The Solar Wind

- Extension of the solar corona
- Frozen-in solar corona composition (mostly protons and alpha particles; 0.1% heavy ions - C, N, O, Si, S, Fe,….)
- At 1 AU, average solar wind properties:

$n \approx 7\ cm^{-3}$, $u \approx 400$ km/s, $T \approx 10$ eV, Mach number $M \approx 10$, $B \approx 10$ nT.

- Slow and fast speed solar wind streams.

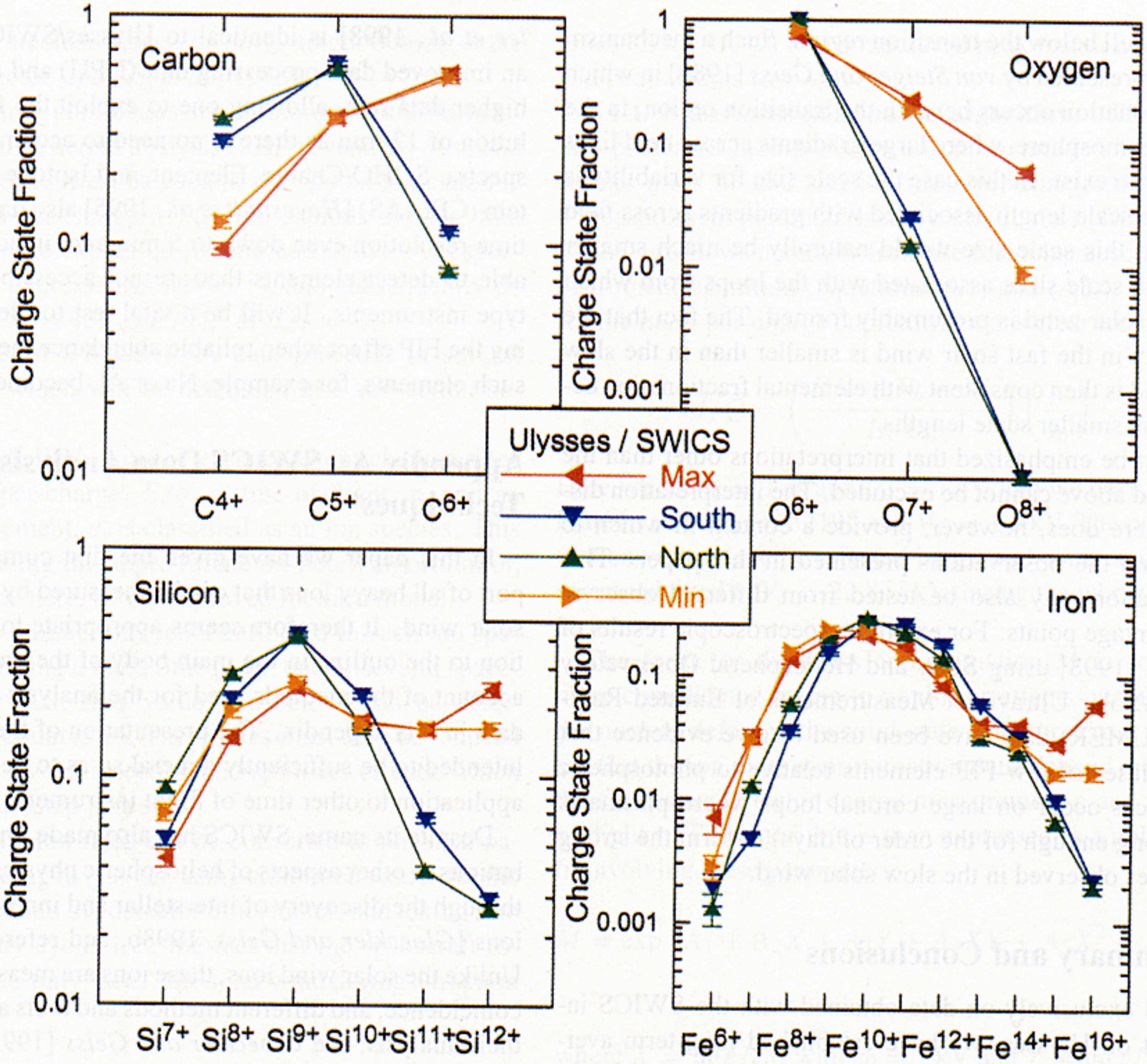

Plate 5. Average charge state spectra of C, O, Si, and Fe from Ulysses/SWICS, obtained during the four ~300-day periods defined in Plate 1. As in Plate 4, data points denote averages of the daily values, but here the bars indicate the errors of the mean values.

Solar Wind Charge Exchange (SWCX) Mechanism for X-Ray Emission

- Solar wind ion M^{q+} (O, N, C, Fe, Si, Ne..)
- Cometary or interstellar neutrals H, He, or H_2O, …..
- Charge transfer collisions:

$$M^{q+} + H \longrightarrow H^{+} + M^{(q-1)+*}$$

$$M^{(q-1)+*} \longrightarrow M^{(q-1)+} + h\nu$$

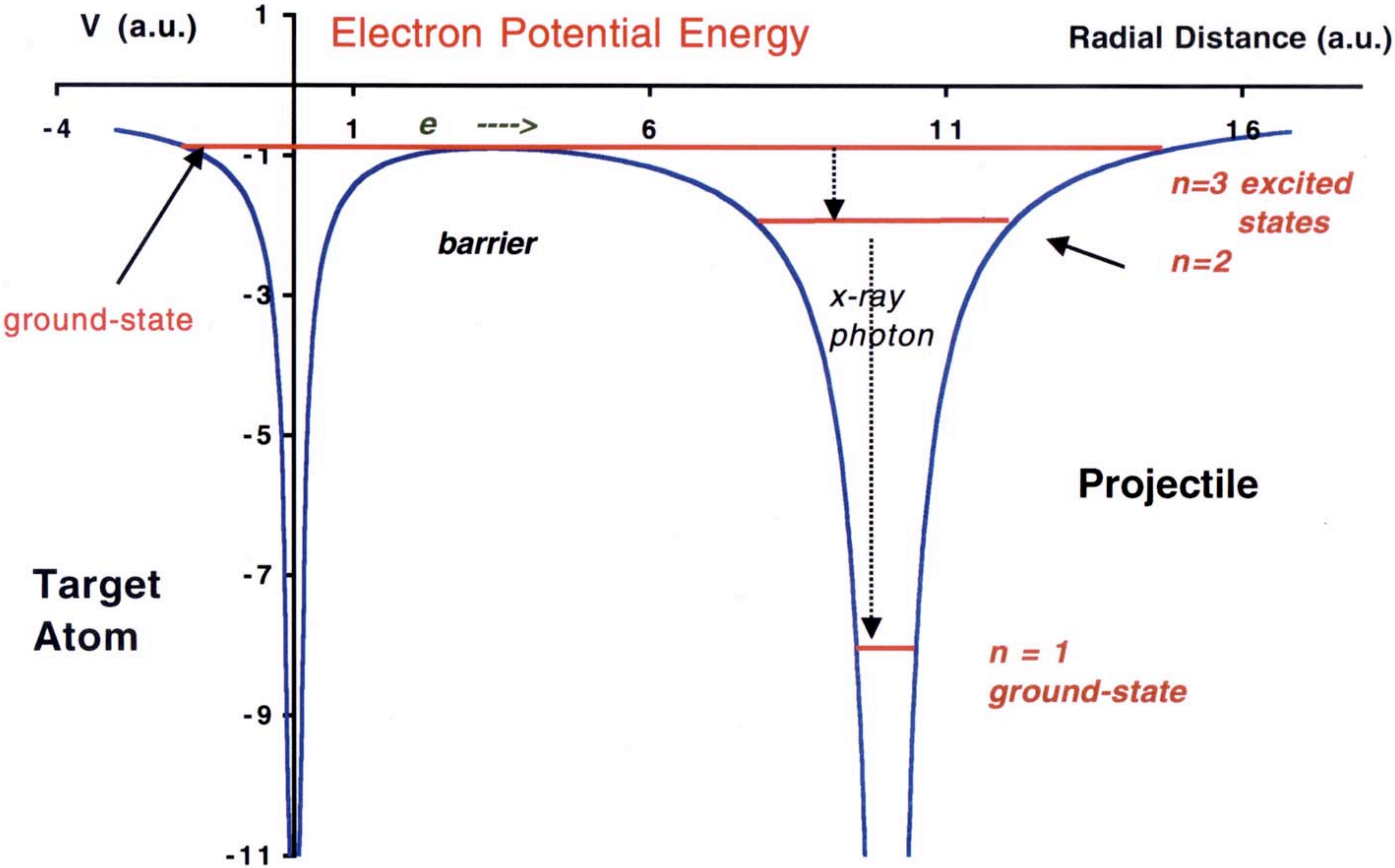

Cravens, 2002

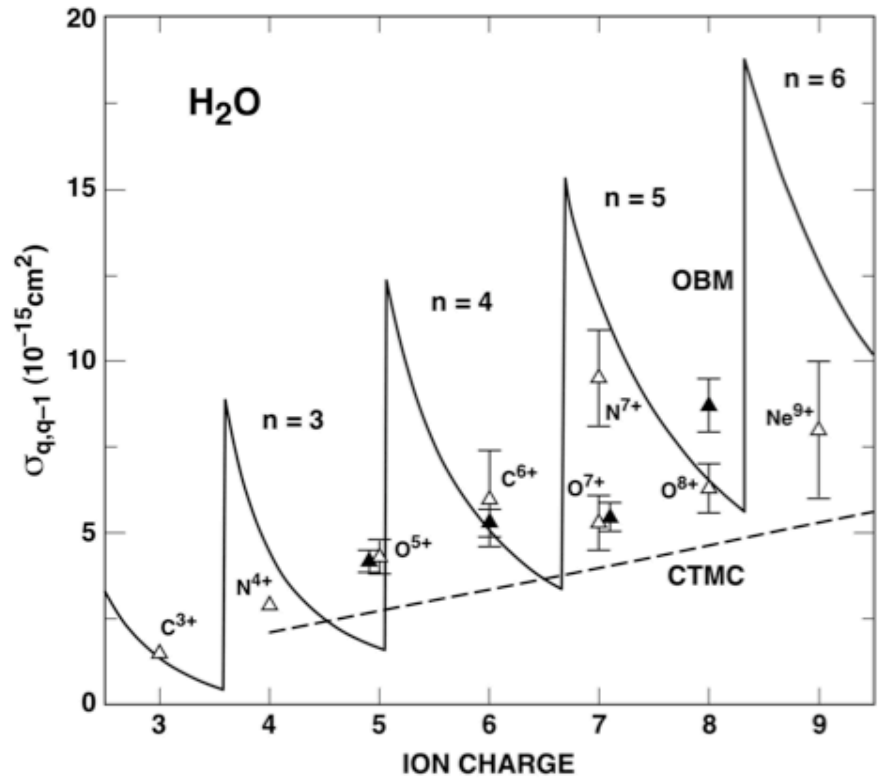

Figure 3

R. J. Mawhorter, A. Chutjian et al. (2007)
Experimental Charge Transfer Cross Section
Measurements at Solar Wind Energies

Experimental Charge-Exchange Cross Sections

Comparison with simple Over Barrier Model and Classical Trajectory Monte Carlo calculations

-- large cross sections!

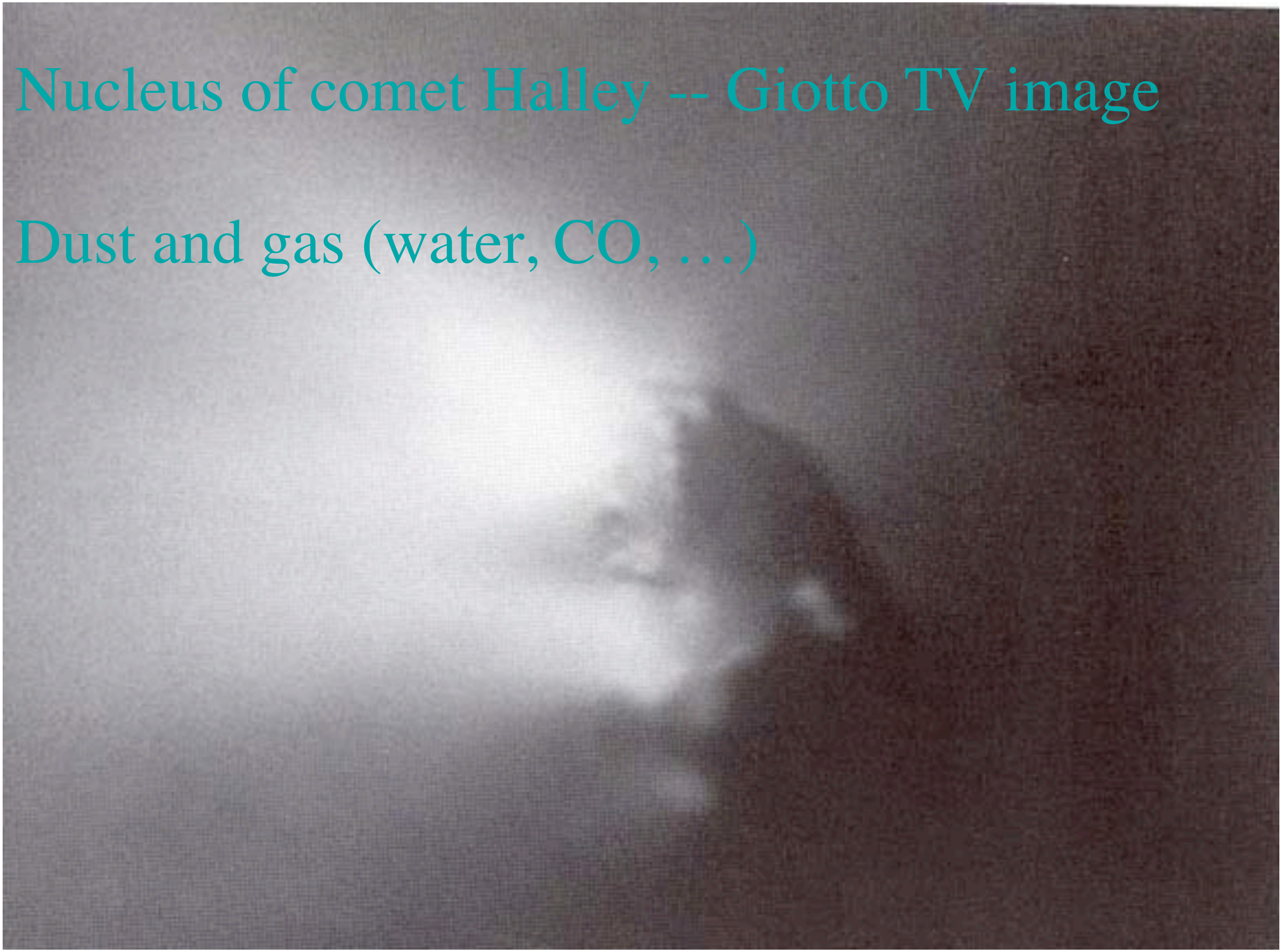
Nucleus of comet Halley -- Giotto TV image
Dust and gas (water, CO, ….)

Chandra image of Comet LINEAR (Lisse et al., 2001)

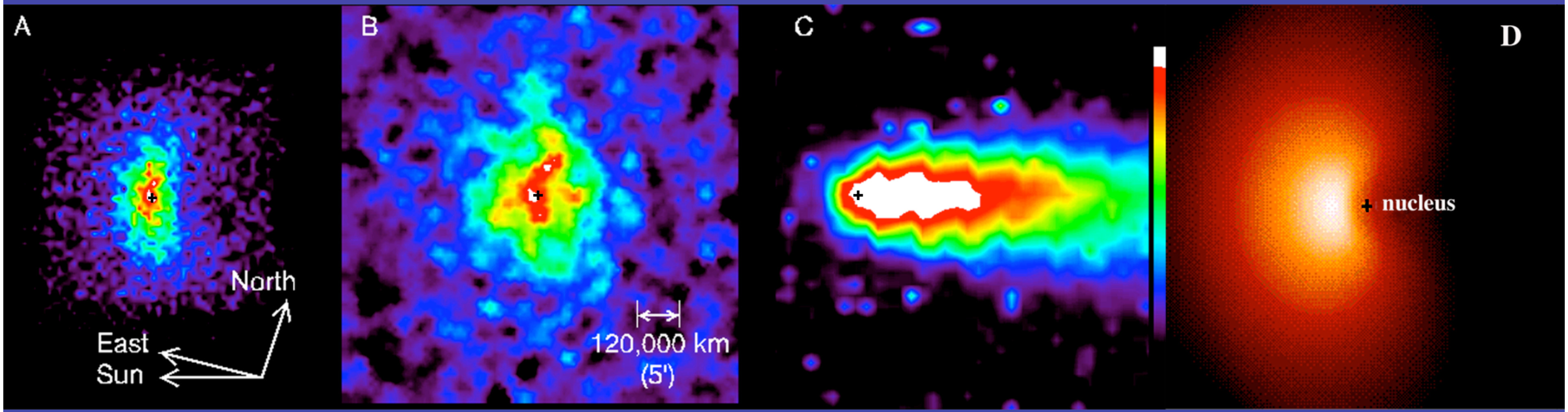

Soft x-rays

EUV

Optical

MHD model

Cometary X-Ray Emission (Power ≈ 1 GW)

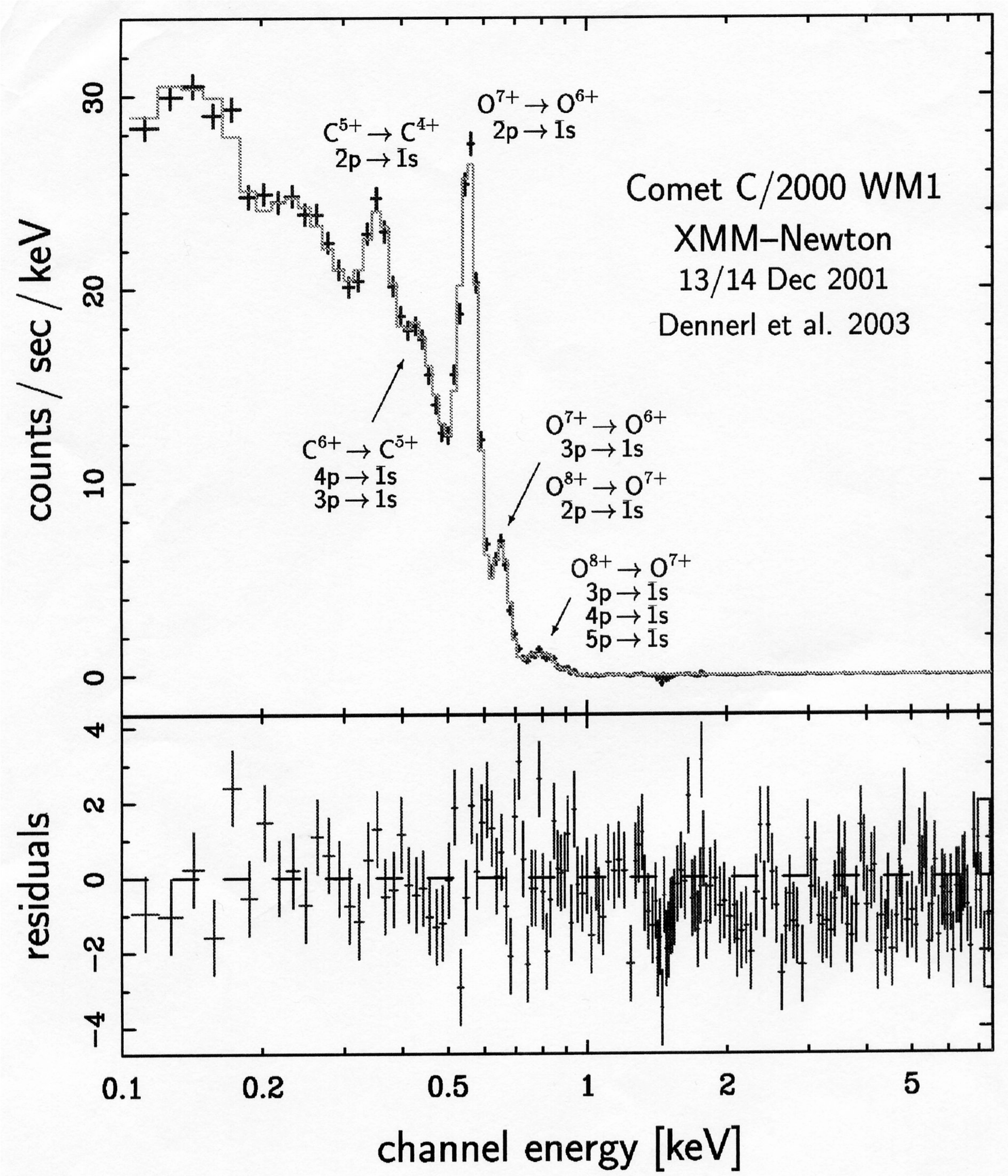

Dennerl et al (2003)

Cometary
X-Ray Spectrum

XMM Newton

X-Ray Emission From the Magnetosheath / Geocorona due to SWCX

- Geocoronal atomic hydrogen extends tens of Earth radii above the surface.
- The shocked solar wind is diverted around the magnetopause.
- The SWCX mechanism operates in the magnetosheath due to collisions with the H.
- Apparently, this has been seen as emission from the dark side of the Moon (ROSAT - Schmidt et al., 1991, and recently CXO -- Wargelin et al. 2004)

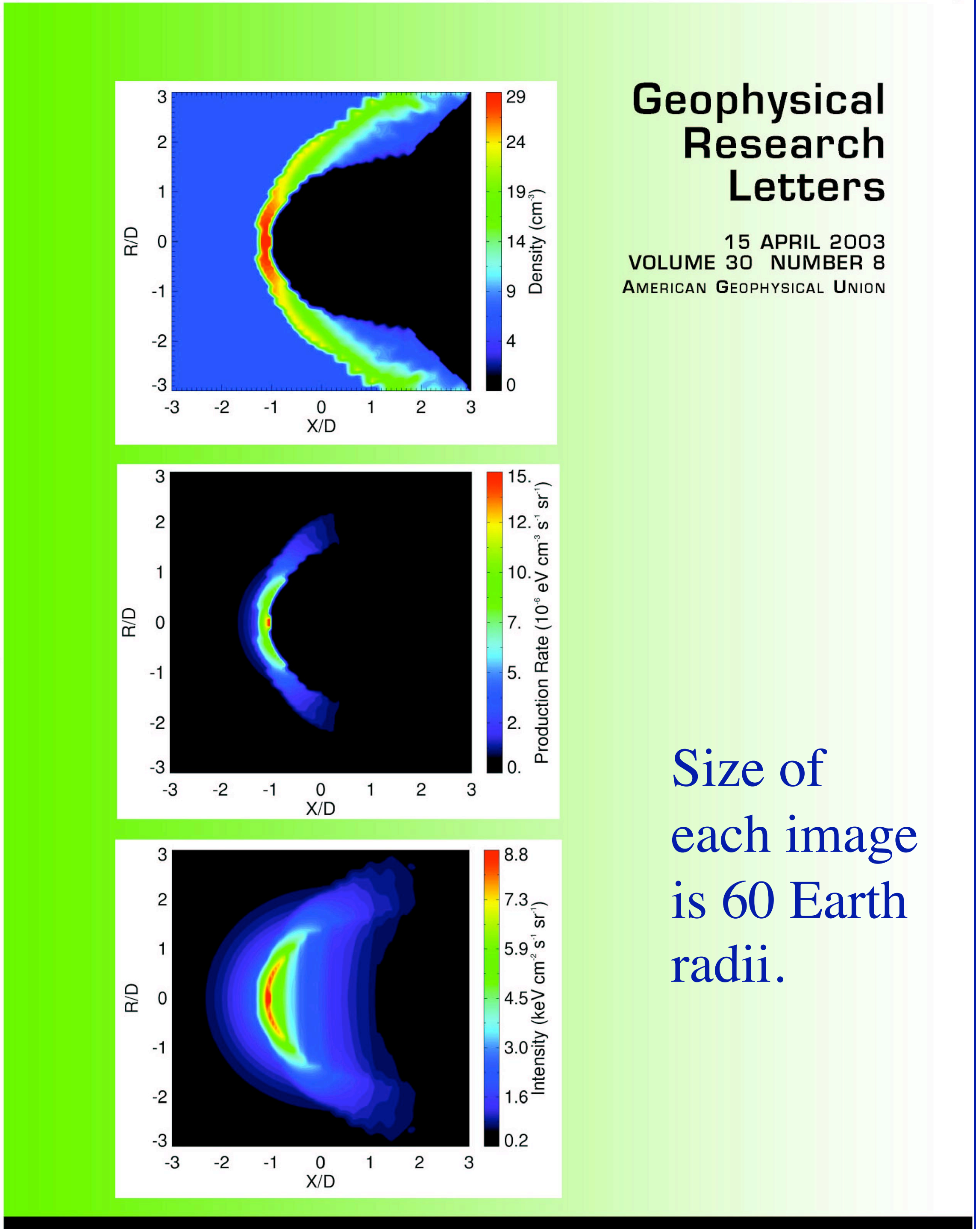

Size of each image is 60 Earth radii.

X-Ray emission from the terrestrial magnetosheath and geocorona due to the SWCX mechanism.

Robertson and Cravens (2003)

ROSAT 1/4 keV x-ray background LTE compared with measured IMP-8 solar wind proton fluxes -- Cravens, Robertson, and Snowden, 2001.

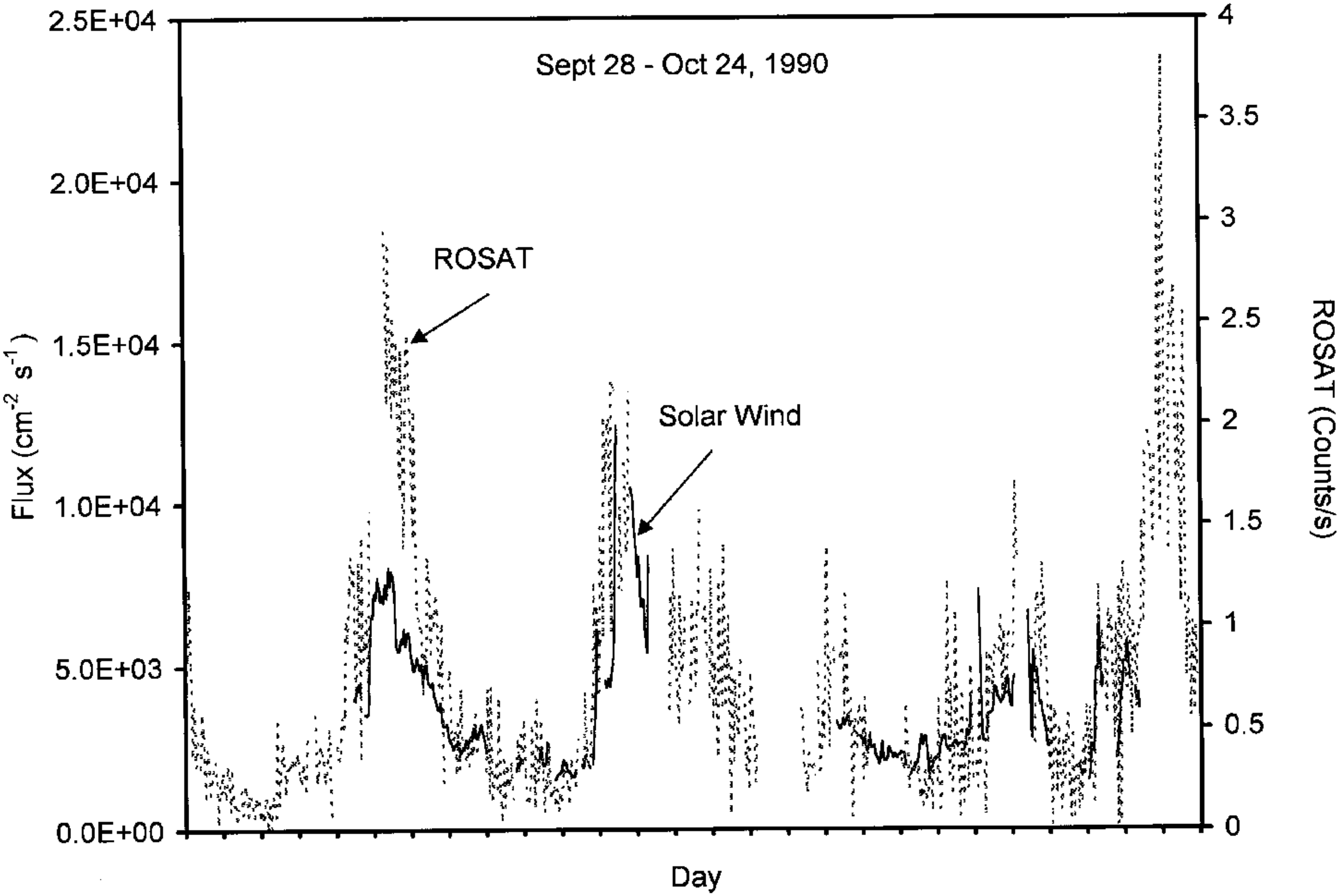

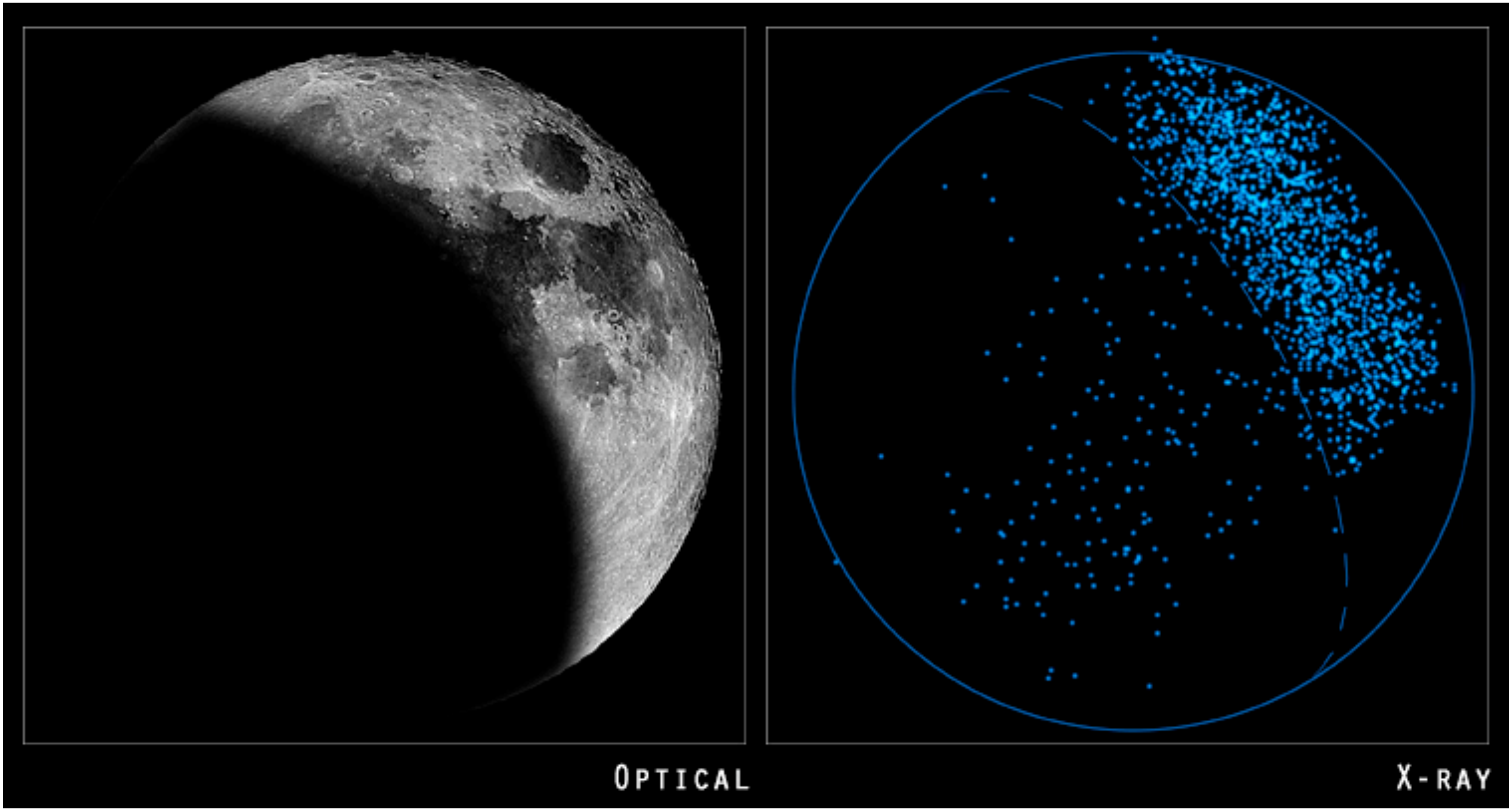

Lunar X-Ray Emission from CXO (Wargelin et al., 2004)

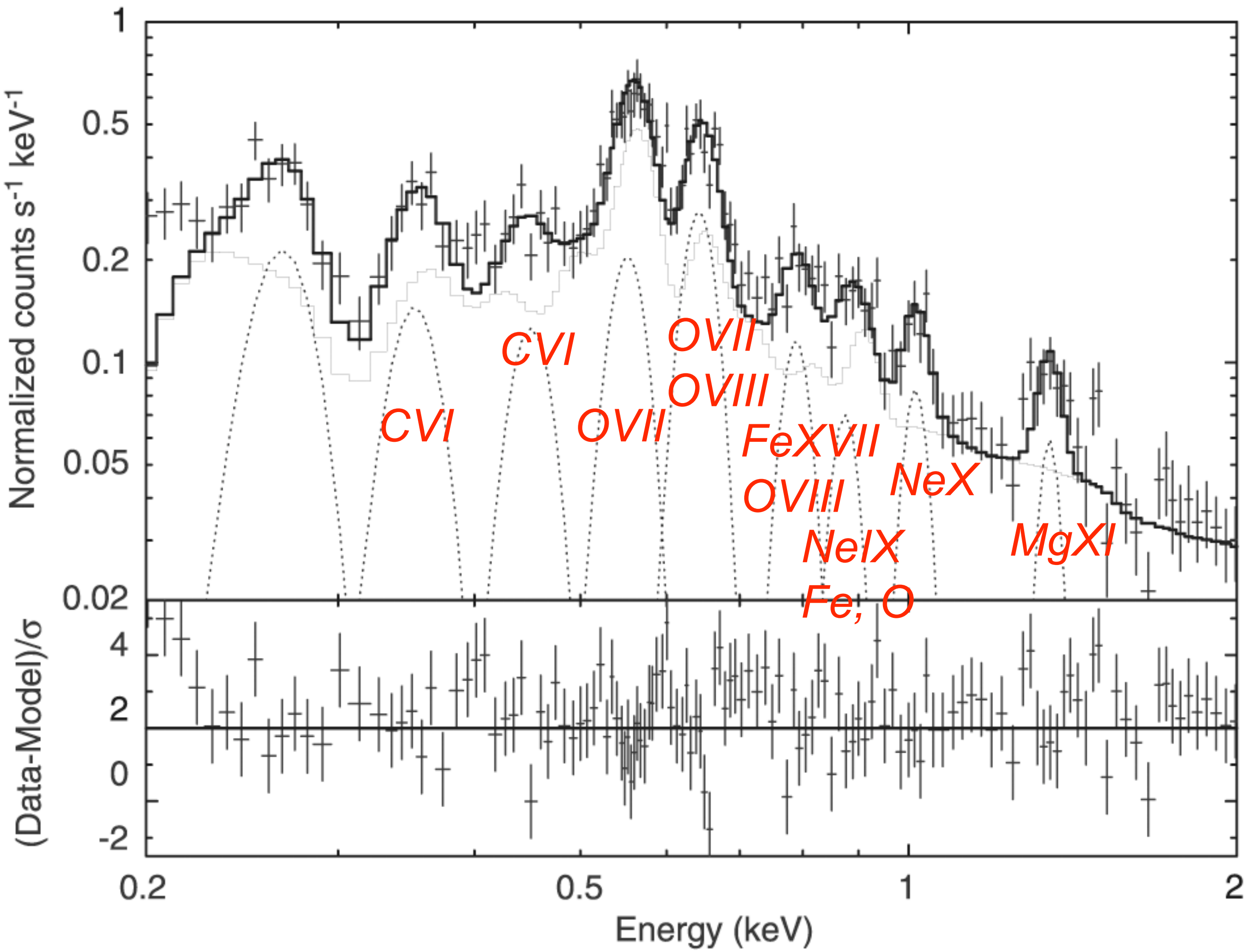

Fujimoto et al. (2007)

Suzaku observations of

magnetosheath X-rays during a solar event/ LTE.

Martian X-Rays observed by XMM-Newton and organized by Spectral Region (Dennerl et al., 2006)

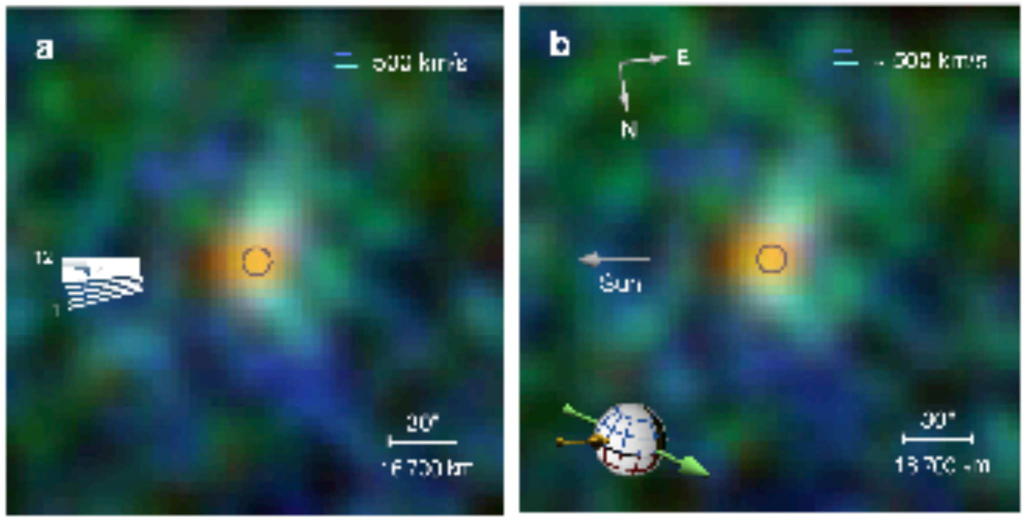

Red -- carbon K -shell (solar fluor.)

Blue -- ionized oxygen (SWCX)

Information provided on solar wind interaction with exosphere of Mars:
Solar wind flow around planet and exospheric neutral density distributions.

Heliospheric X-Ray Emission

- From SWCX mechanism applied to solar wind interaction with interstellar neutral H and He streaming into the heliosphere (Cox, 1998; Cravens, 2000).
- Spectrum is consistent with observed soft x-ray background emission (rockets, ROSAT…)

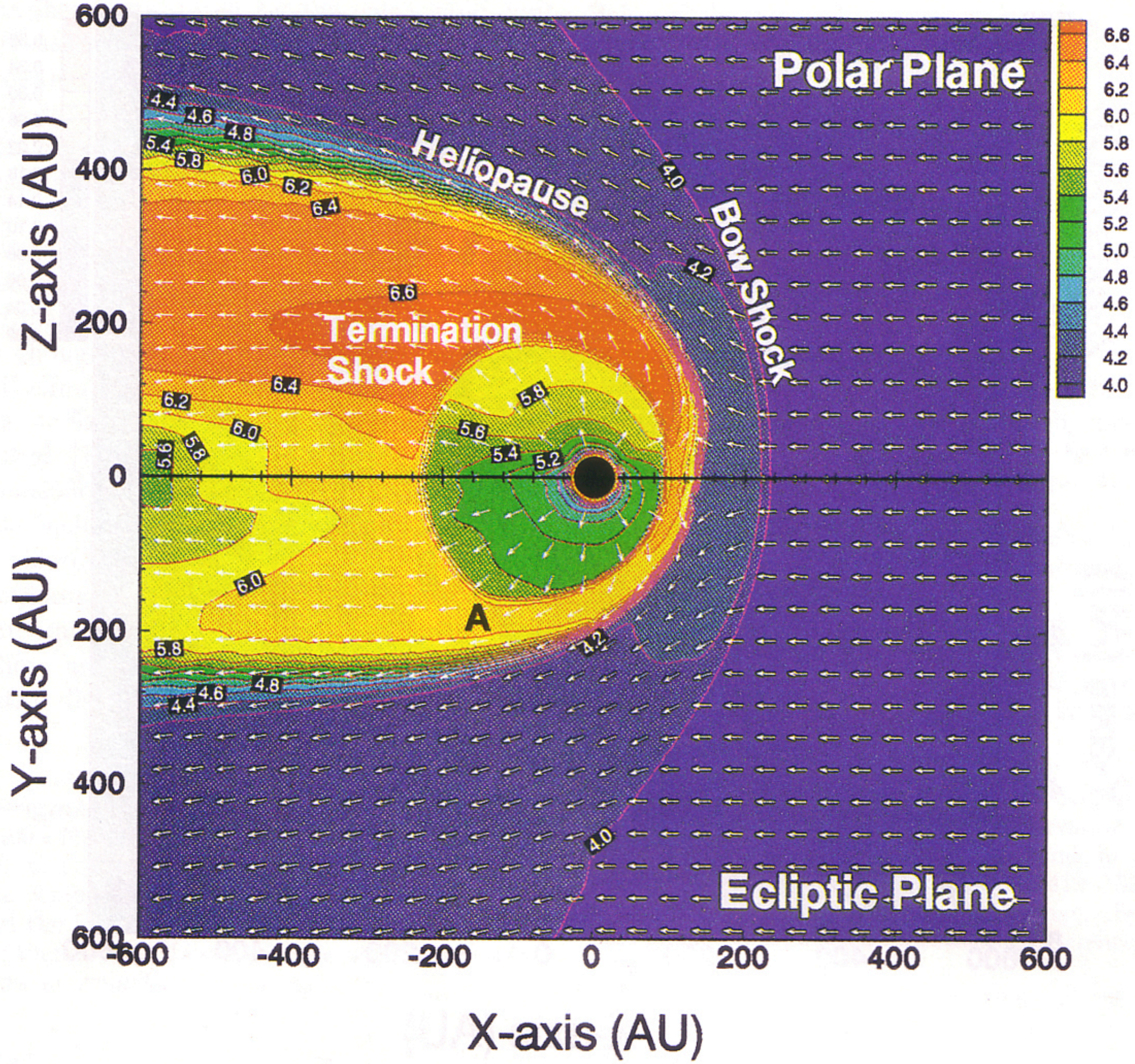

Plate 1. Log[proton temperature (K)] (contour and color) and normalized flow vectors as a function of distance in the polar plane (top panel) and in the ecliptic plane (bottom panel). The position of a triple point in the flow is shown by the letter A.

Pauls and Zank (1997) 2-fluid model of heliosphere and ISM

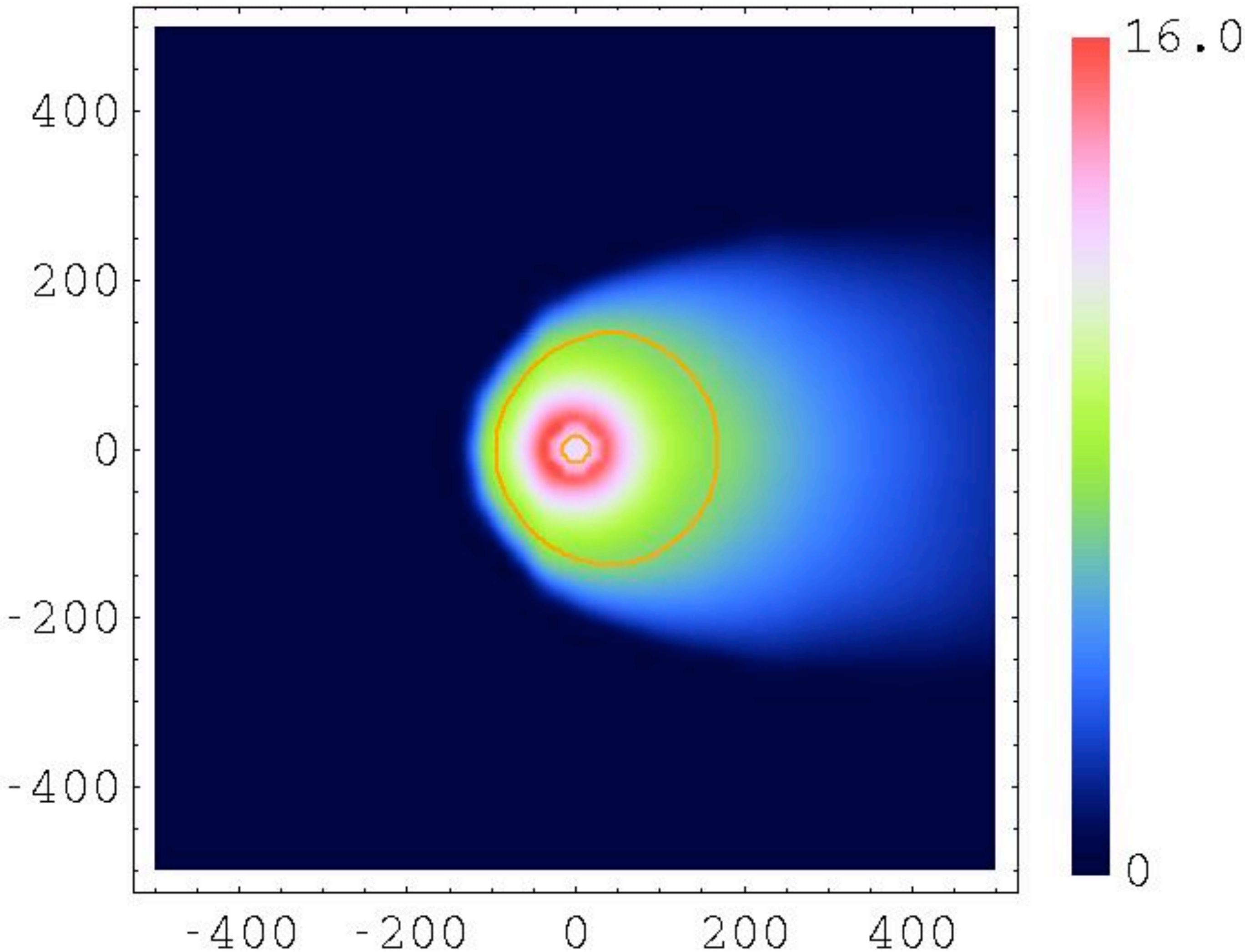

Modeled X-ray map for O^{7+} ---> O^{6+}. Units are photons/cm^2/s.

Medvedev et al. (2006)

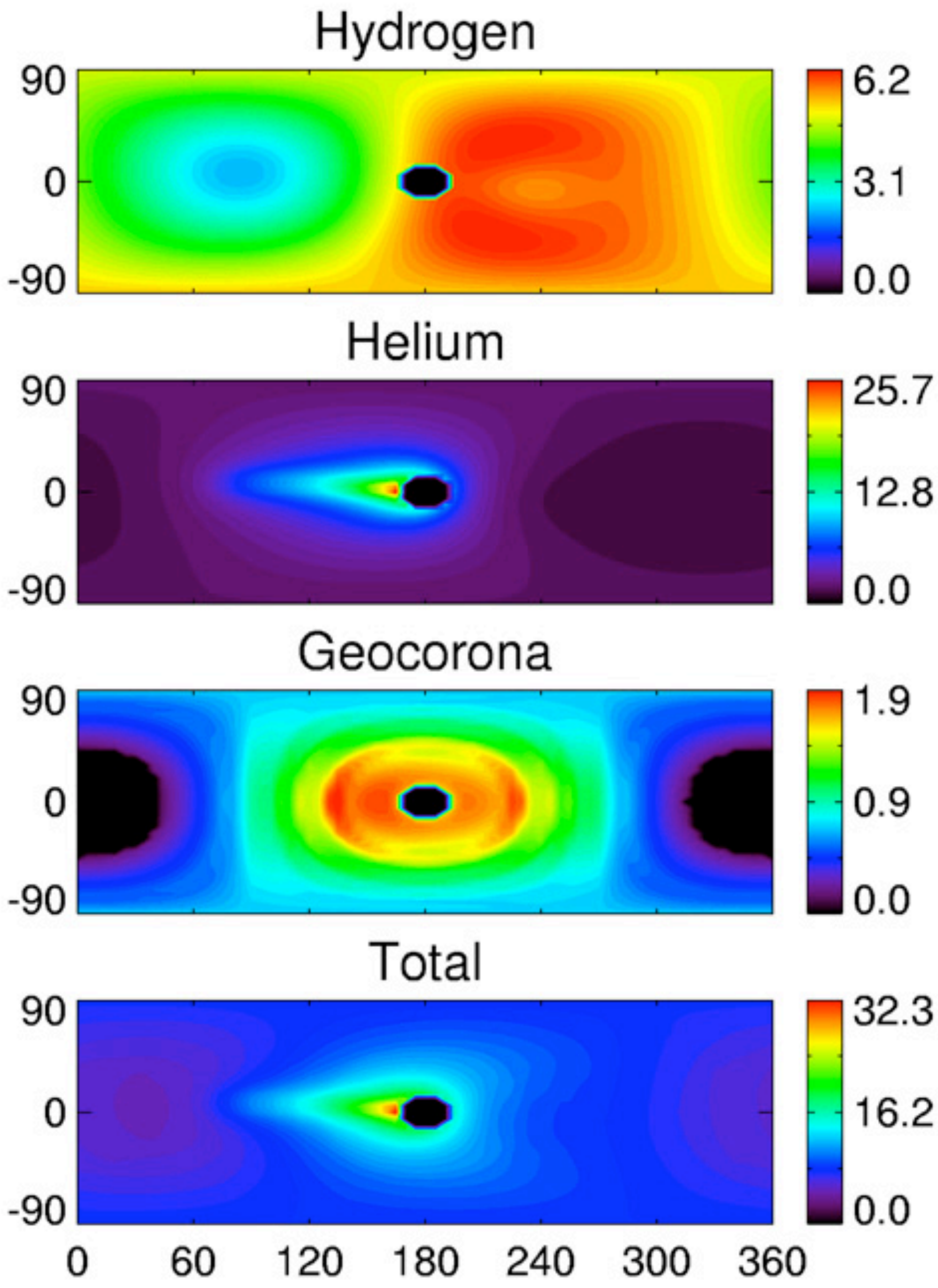

Robertson, Cravens, Snowden (2003)

Predicted heliospheric (interstellar neutrals) and geocoronal x-ray emission versus look direction.

(Earth-centered Heliolatitude and longitude.)

Note the helium “cone”.

From Henbest and Cooper (1994).

120 pc by 120 pc

View in the galactic plane of the nearby interstellar medium (***the local bubble***).

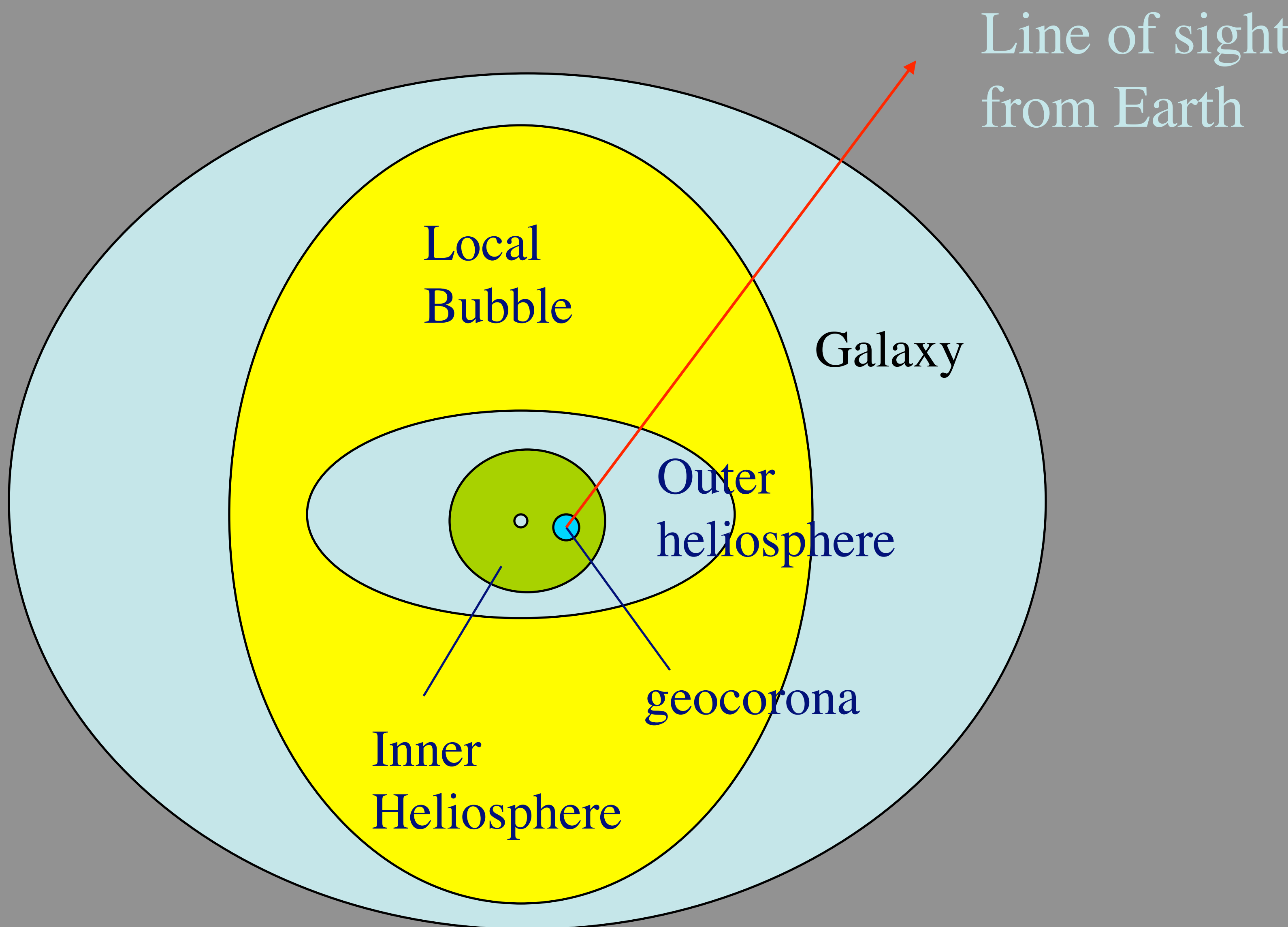

REGIONS EMITTING SOFT X-RAYS (contributions to the observed soft x-ray background (SXRB))

Possible Ways to Purge the SXRB of SWCX Contributions

- Spatial/directional morphology.
- Temporal variability (already partially successful - LTE removal).
- Spectral differences (such as line ratios) - potentially powerful but high resolution needed.
- Modeling combined with above.

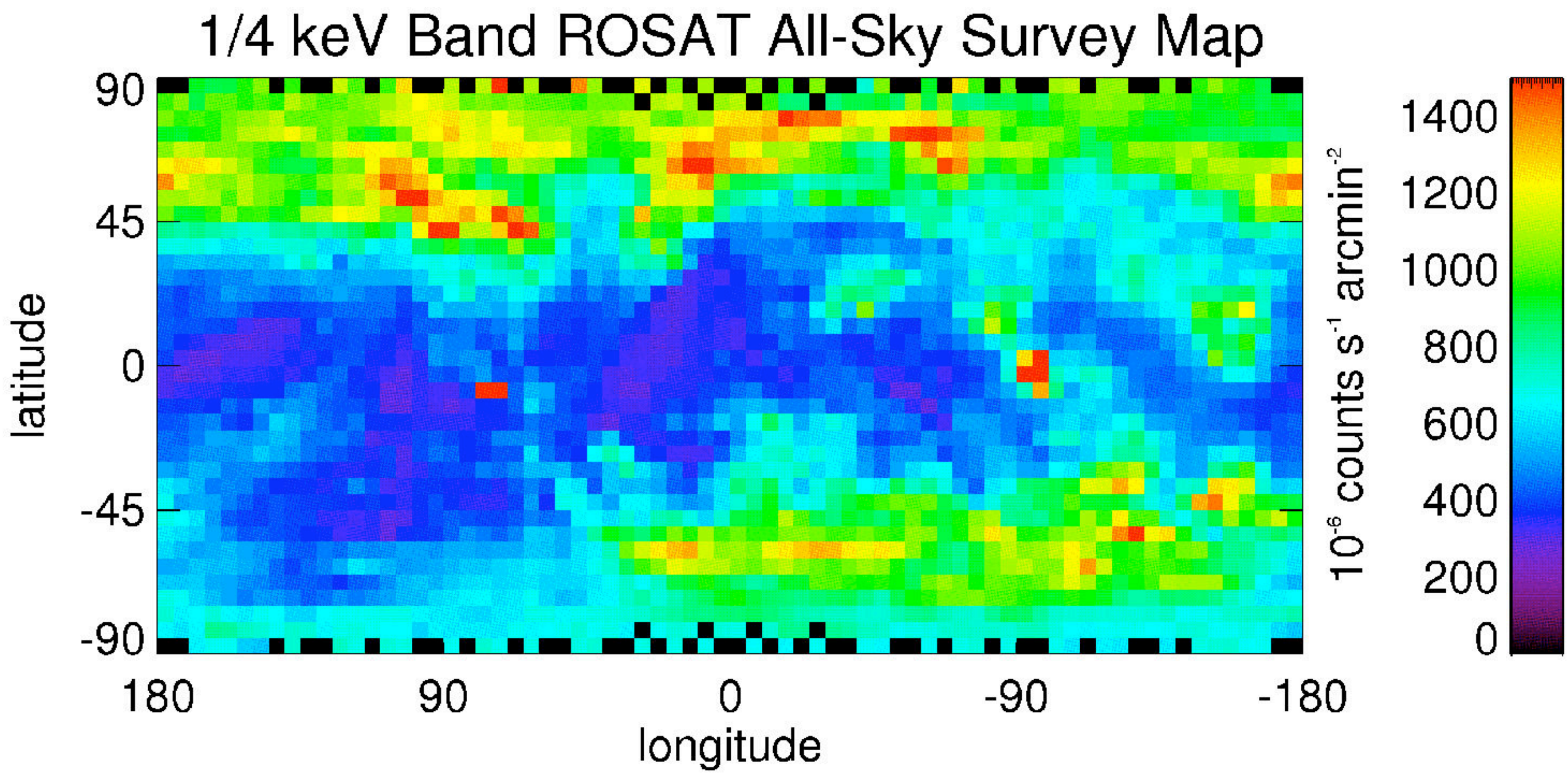

1/4 keV Band ROSAT All-Sky Survey Map
90
45
0
-45
-90
latitude
180
90
0
-90
-180
longitude
10-6 counts s-1 arcmin-2
1400
1200
1000
800
600
400
200
0

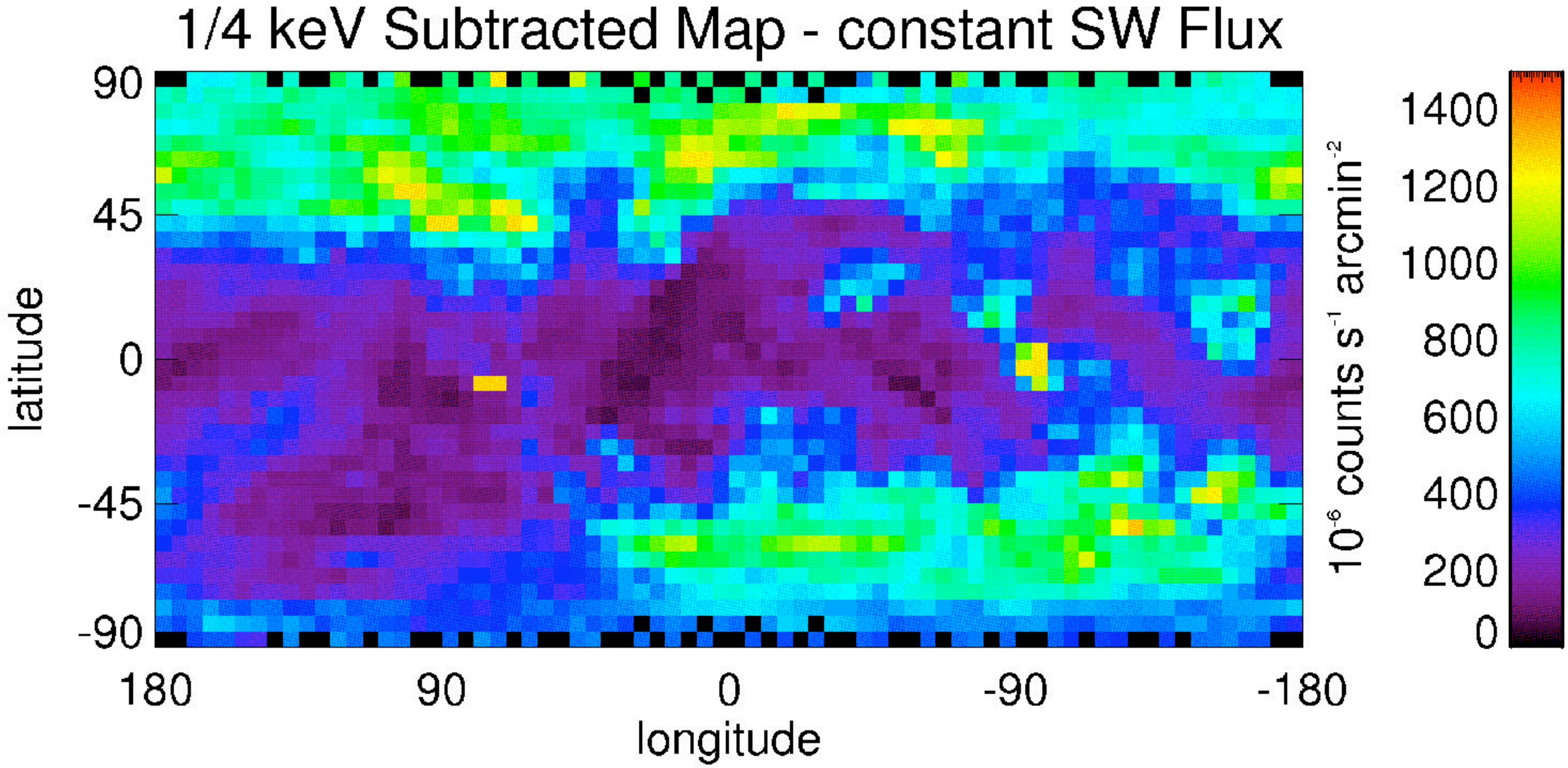
1/4 keV Subtracted Map - constant SW Flux
latitude
90
45
0
-45
-90
180
90
0
-90
-180
longitude
10^{-6} counts s^{-1} $arcmin^{-2}$
1400
1200
1000
800
600
400
200
0

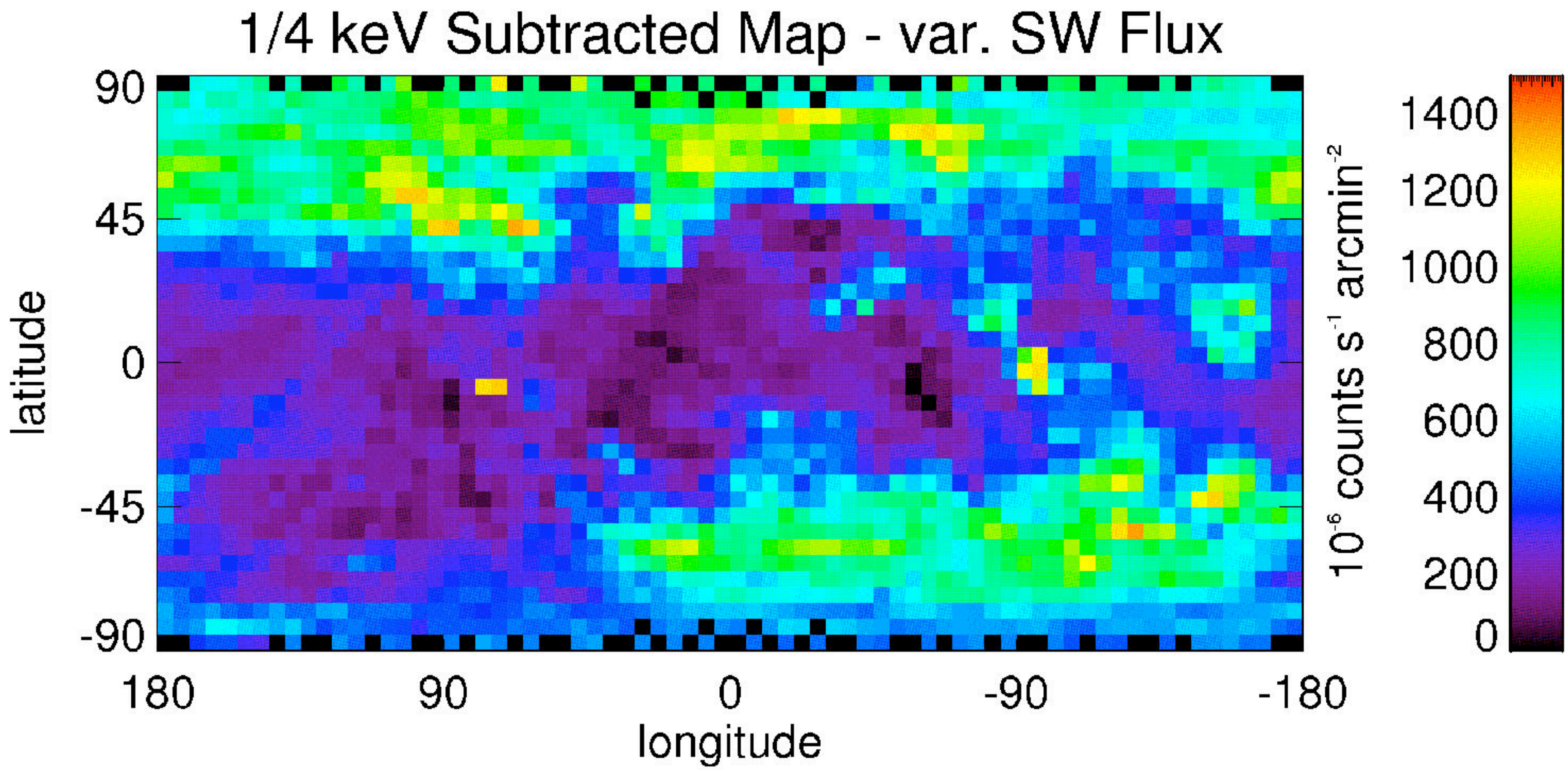
1/4 keV Subtracted Map - var. SW Flux
90
45
0
-45
-90
latitude
180
90
0
-90
-180
longitude
10^{-6} counts s^{-1} $arcmin^{-2}$
1400
1200
1000
800
600
400
200
0

Use the spectrum to distinguish standard collisional from SWCX?

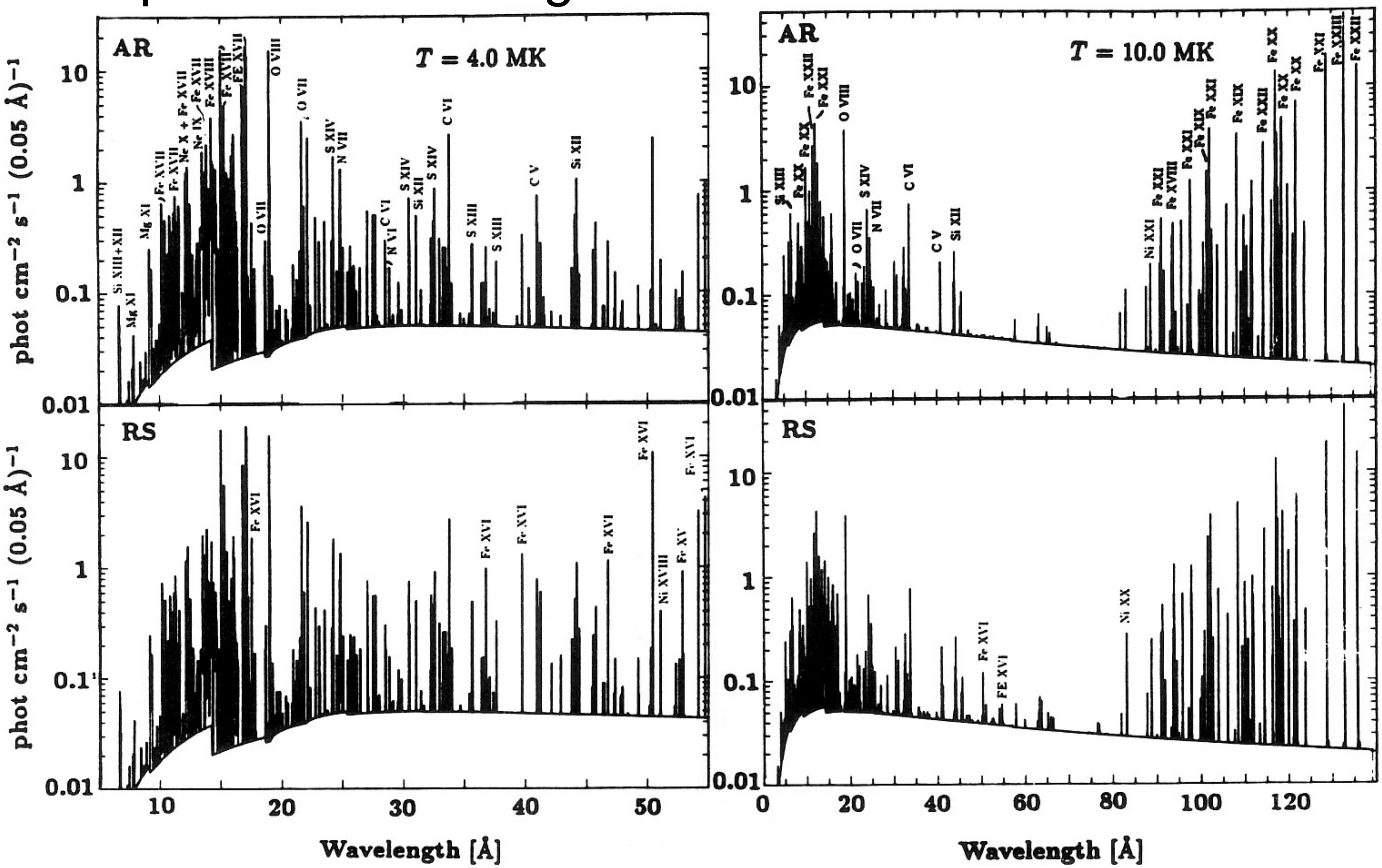

Figure 5b. Comparison of AR and RS calculated spectra for $T = 4$ and 10 MK in the wavelength regions 5–55 Å and 3–140 Å, respectively.

From Mewe et al. (1990). Hot plasma - lines and more lines

Collisional due to electrons. Similar to SWCX spectrum.

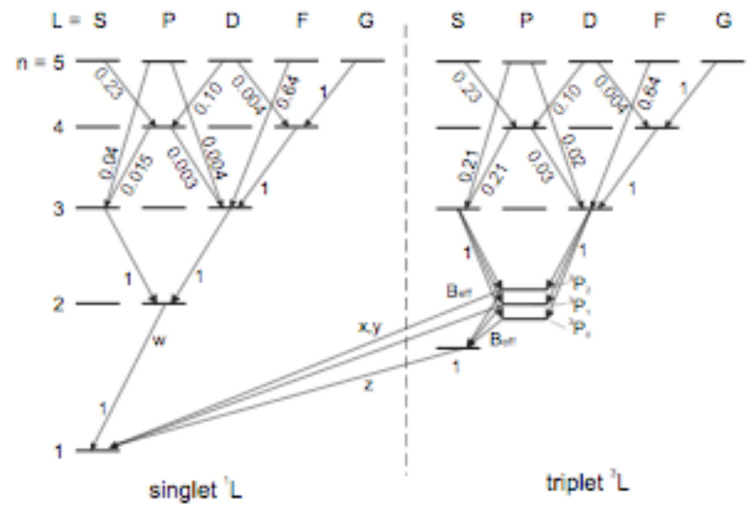

Figure 7.1: *Part of the decay scheme of a helium-like ion.*

Table 7.1: *Apparent effective branching ratios, B_{eff}, for the decay of the 2^3P state of He-like carbon and oxygen ions.*

transition	CV	OVII
1^1S_0–$2^3P_{1,2}$	0.11	0.30
2^3S_1–$2^3P_{0,1,2}$	0.89	0.70

sumed statistical population of the triplet P-term:

$$B_{eff} = \sum_{j=0}^{2} \frac{(2j+1)}{(2L+1)(2S+1)} \cdot B_j \qquad (7.5)$$

The resulting effective branching ratios are given in Table 7.1.

The ratio G is not equal to the overall triplet-to-singlet ratio, because in the singlet system the np-states decay to the ground state directly. G thus depends both on the triplet to singlet ratio, and on the initial distribution over the $n\ell$ states.

7.2 Analysis

7.2.1 C^{5+}

Charge exchange spectra following C^{5+}+H_2O collisions are complex and contain many emission lines. Equipped with a 1200 grooves/mm grating, our EUV spectrometer has a

Bodewits Ph. D. Thesis (2007)

Helium-Like ion spectrum

OVII line complex near 560 eV.

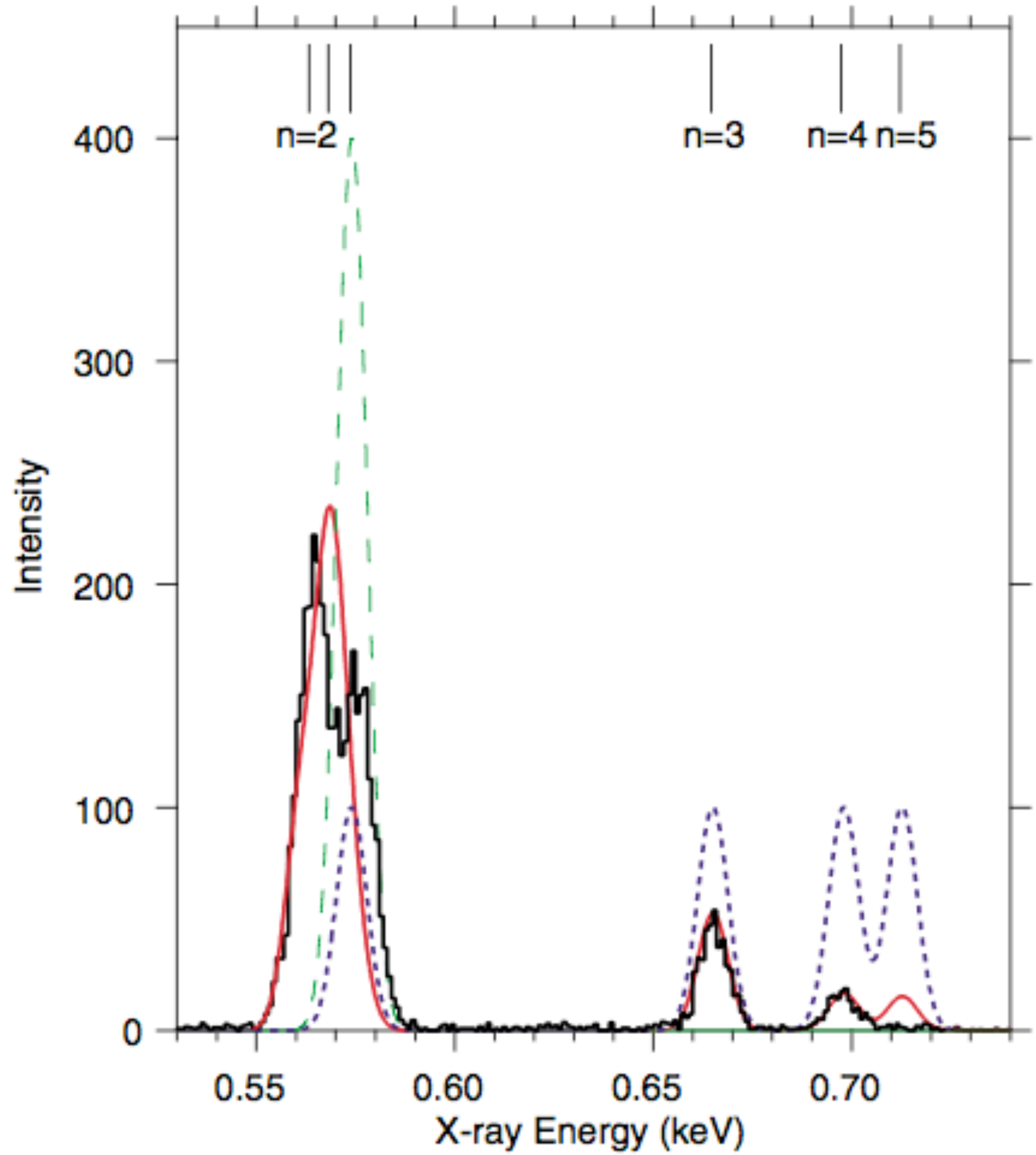

Laboratory Simulation of Charge Exchange produced X-Ray Emission from Comets using the Spare *ASTRO-E* Microcalorimeter
P. Beiersdorfer et al. (2003)

Güdel et al. (2007) Science
Orion Extended Nebula X-Ray Emission

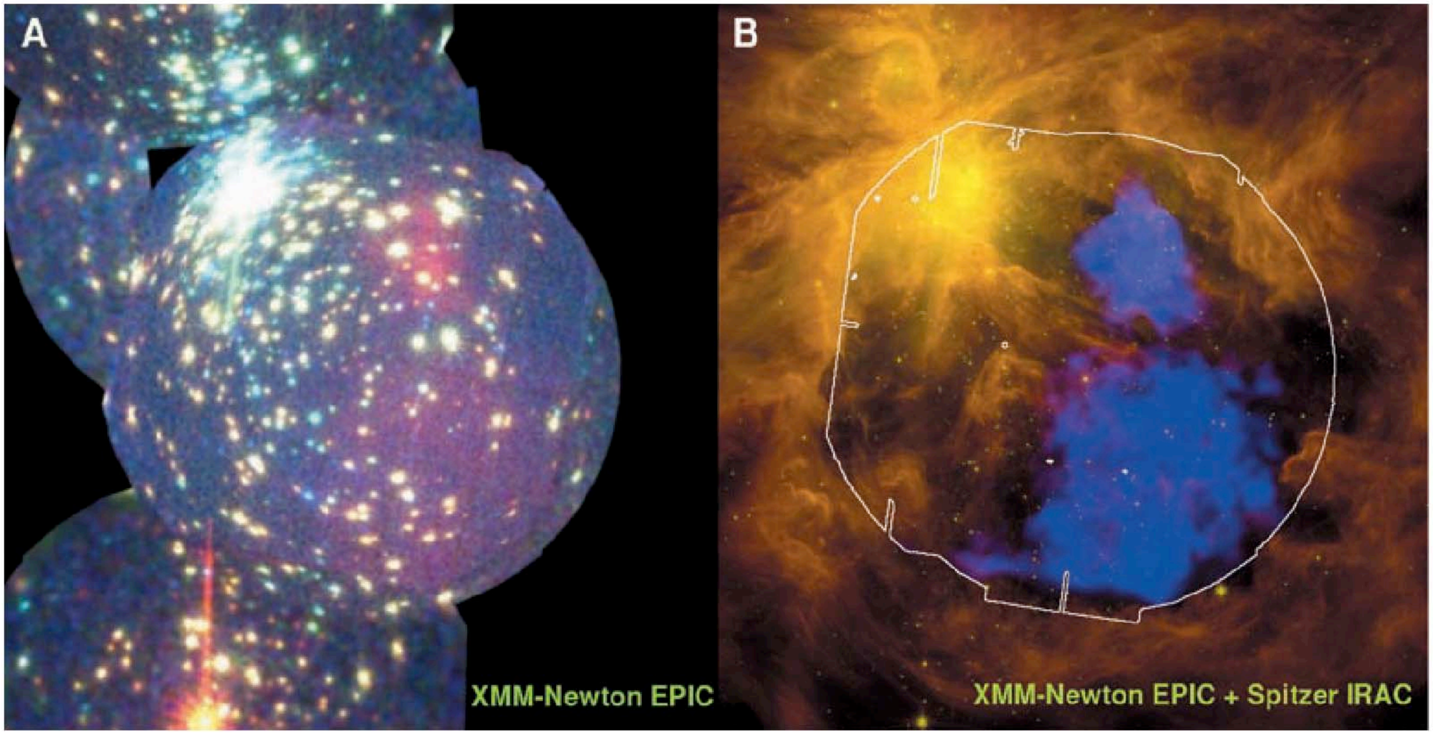

Fig. 2. The Orion Nebula with its hot gas bubble. The x-ray image (**A**) is color-coded for photon energies in the 0.3 to 7.3 keV range (red to blue). The diameter of each of the near-circular fields is 30 arc min (3.5 pc), and the angular resolution is about 5 arc sec. (**B**) On the same scale, the excess diffuse emission in the 0.3- to 1-keV band with respect to the hard band extracted from the longest observation (*16*) in blue, overlaid on a composite 4.5-μm (green channel) and 5.8-μm (red channel) mid-infrared image from the Spitzer Space Telescope. X-ray point sources have been removed, and the residual image has been adaptively smoothed (*16*). The intensity scale is logarithmically compressed. The white contour shows the detector field of view for this x-ray observation. IRAC, Infrared Array Camera. North is up, and west is to the right.

The blue designates a soft x-ray emission region (XMM Newton)
The scale is a few parsecs.

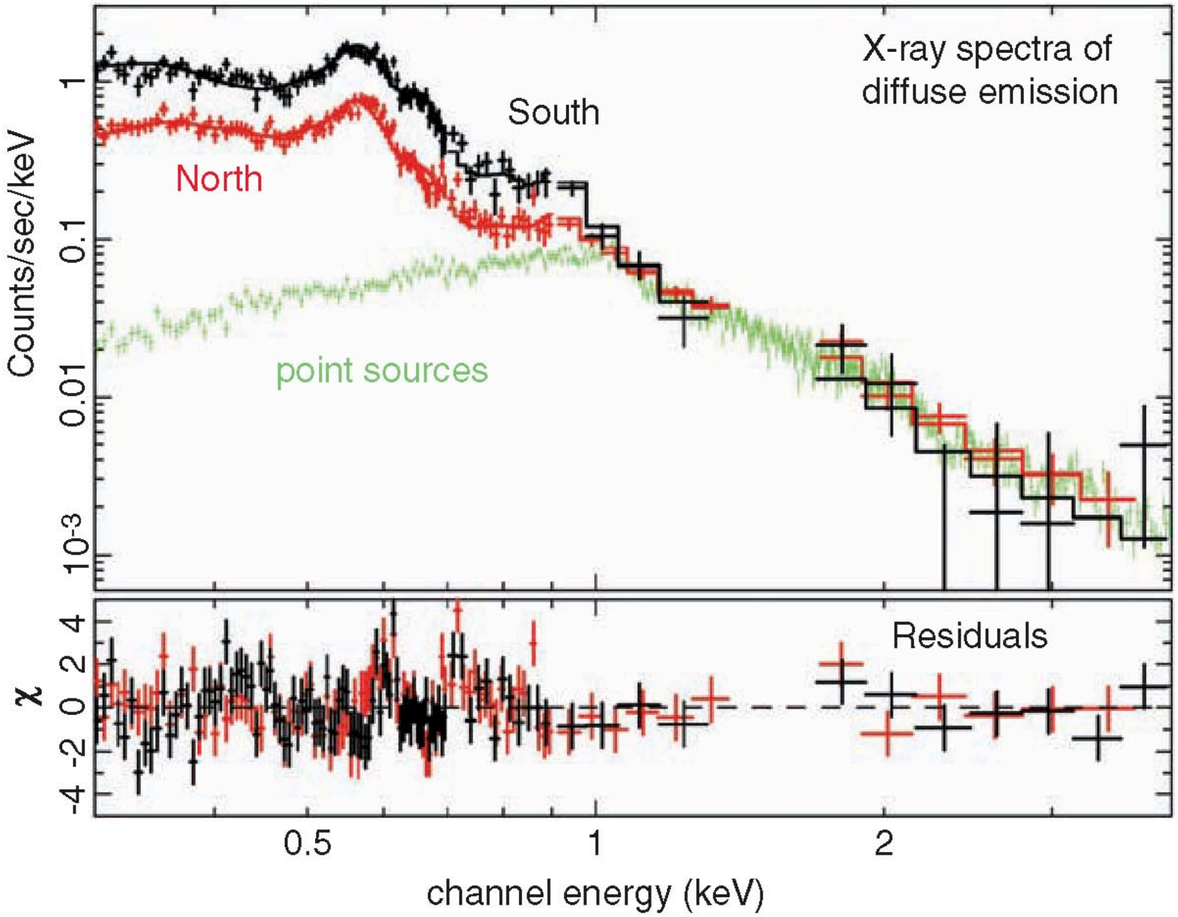

Fig. 3. X-ray spectra of the diffuse emission. The red and black spectrum refer to, respectively, the northern bright patch and the southern more-extended structure in Fig. 2. The error bars attached to each data point reflect 1σ errors from counting statistics. The solid histograms represent a model fit to the spectra on the basis of emission from a thermal plasma (*16*). The bottom graph gives the fit residuals. The green spectrum shows the contribution from stellar x-rays to the spectrum of the northern diffuse emission.

Güdel et al. (2007) - XMM spectrum of the soft x-rays from the Extended Orion Nebula showing OVII lines near 560 eV.

A SWCX Contribution?

Probably *not*, but it cannot be dismissed out of hand.

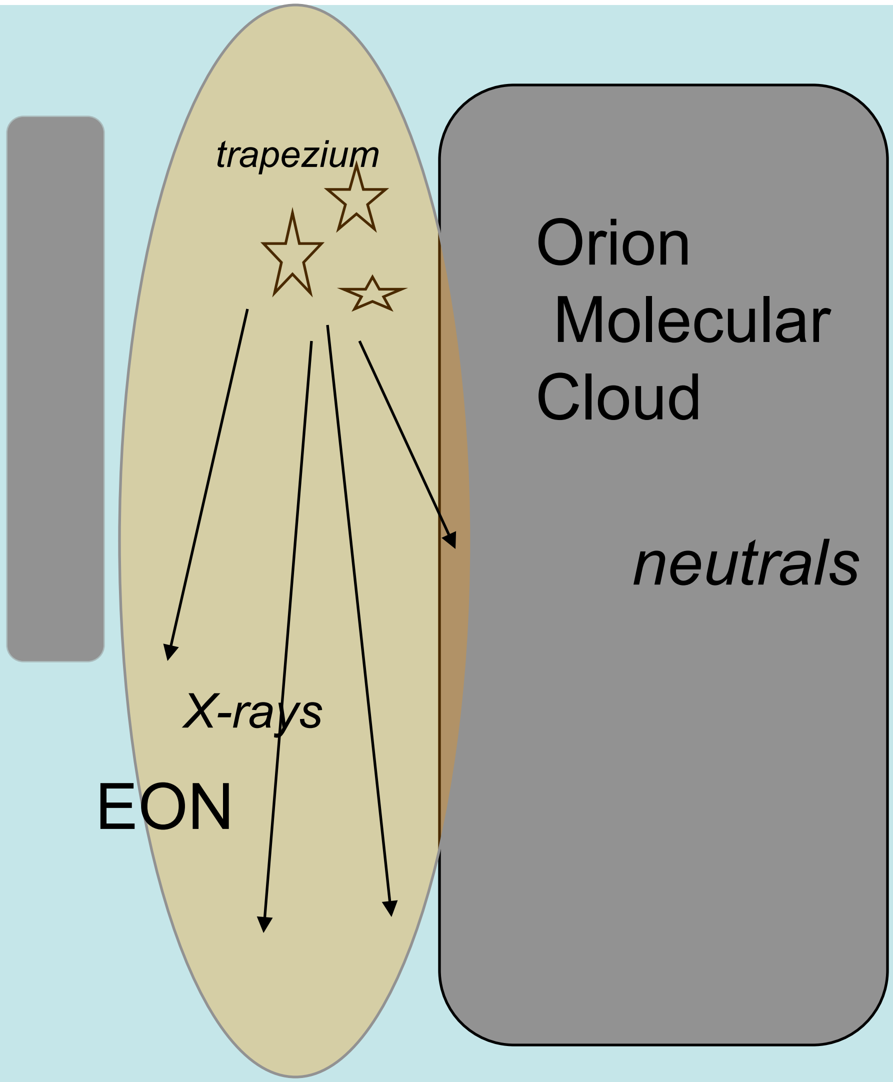

Schematic of plasma outflow in the extended Orion nebula and an area of possible charge exchange X-ray emission.

Summary

- Traditionally x-ray emission has been a diagnostic tool for hot plasmas (e.g., solar corona, supernova remnants, intragalactic medium…).
- Some types of X-ray emission in the solar system can be a diagnostic tool for plasma interactions with neutrals (solar wind - comet/ Earth/heliosphere, auroral x-rays,…)
- The *charge exchange mechanism* has been shown to be particularly important for solar system x-ray emission and might also have applications to *astrophysical plasmas*.

Wargelin et al. (2004)
CXO X-Ray Spectrum of Dark Side of Moon
(geocoronal x-rays) -- looks like SWCX x-rays.

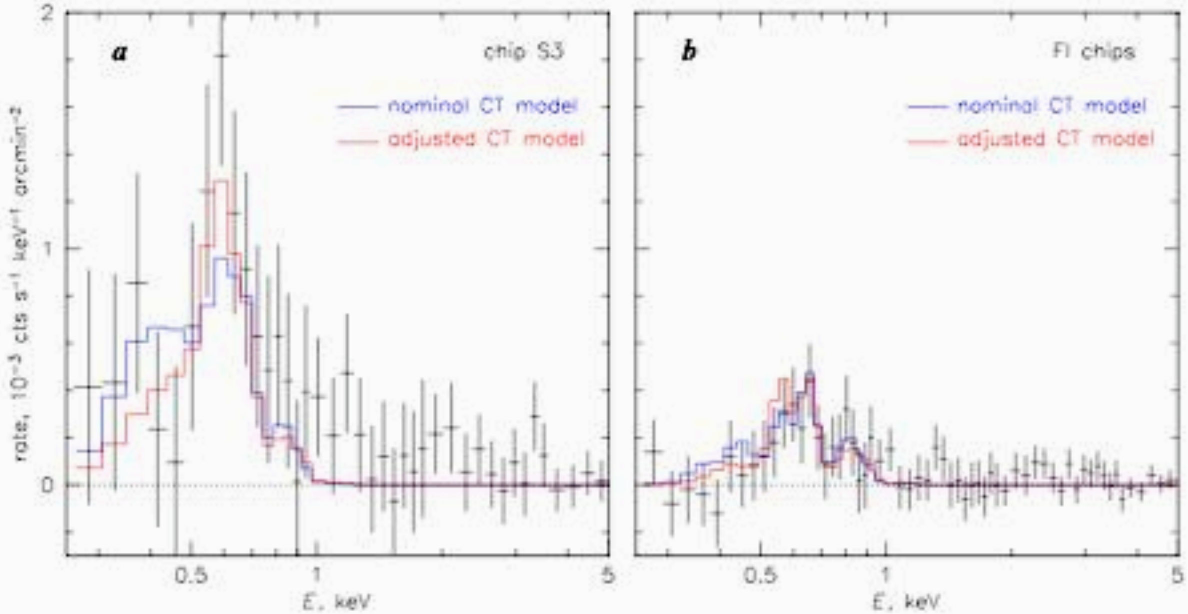

Fig. 6.— Background-subtracted September spectra (3 brightest ObsIDs) and charge transfer model fits using four composite lines. The same model, including normalization, is used to fit the S3 and FI spectra. The nominal fit uses the average (baseline) solar-wind parameters discussed in the text. In the adjusted fit, the relative C VI vs O VII Kα emission is 1/6 of the nominal case, and O VIII emission is reduced by half. Results for the adjusted fit are listed in Table 7.

X-Ray Transitions

- O^{5+} ($1s^2 5d$ --> $1s^2 2p$) 106.5 eV
- O^{6+} ($1s2p$ --> $1s^2$) 568.4 eV
- O^{6+} ($1s2s$ --> $1s^2$) 560.9 eV
- O^{7+} ($2p$ --> $1s$) 654 eV
- C^{5+} ($2p$ --> $1s$) 367.3 eV
- C^{5+} ($4p$ --> $1s$) 459.2 eV

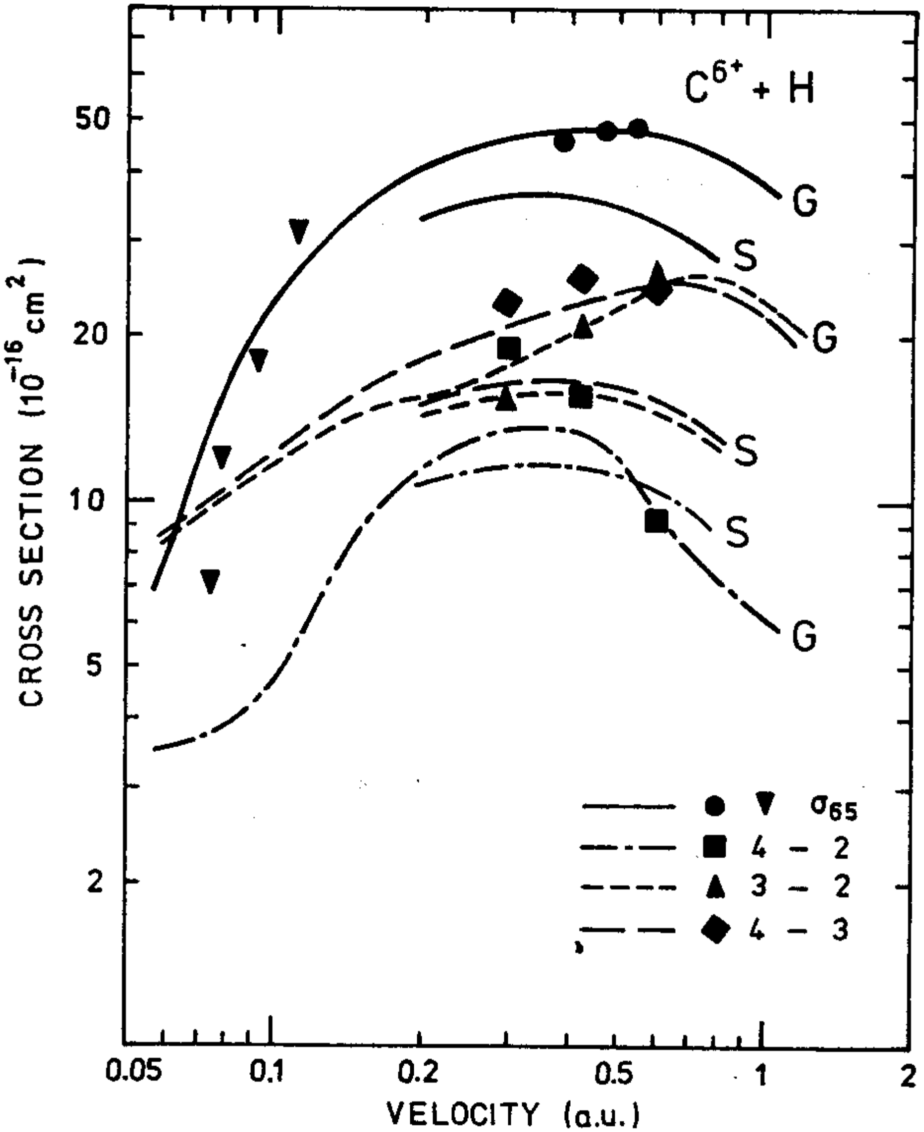

FIG. 18. Total capture cross sections σ_{65} and line-emission cross sections $\sigma_{em}(n - n')$ for C^{6+} in H measured by Dijkkamp *et al.* (1985) using PES. (●), (■), (▲), (◆), Dijkkamp *et al.* (1985); (▼), Phaneuf *et al.* (1982); long curves (G)—theory, Green *et al.* (1982); short curves (S)—theory, Salin (1984).

Fully stripped carbon ion projectiles

Large cross sections

Initial n ≈ 4

Janev, 86 review

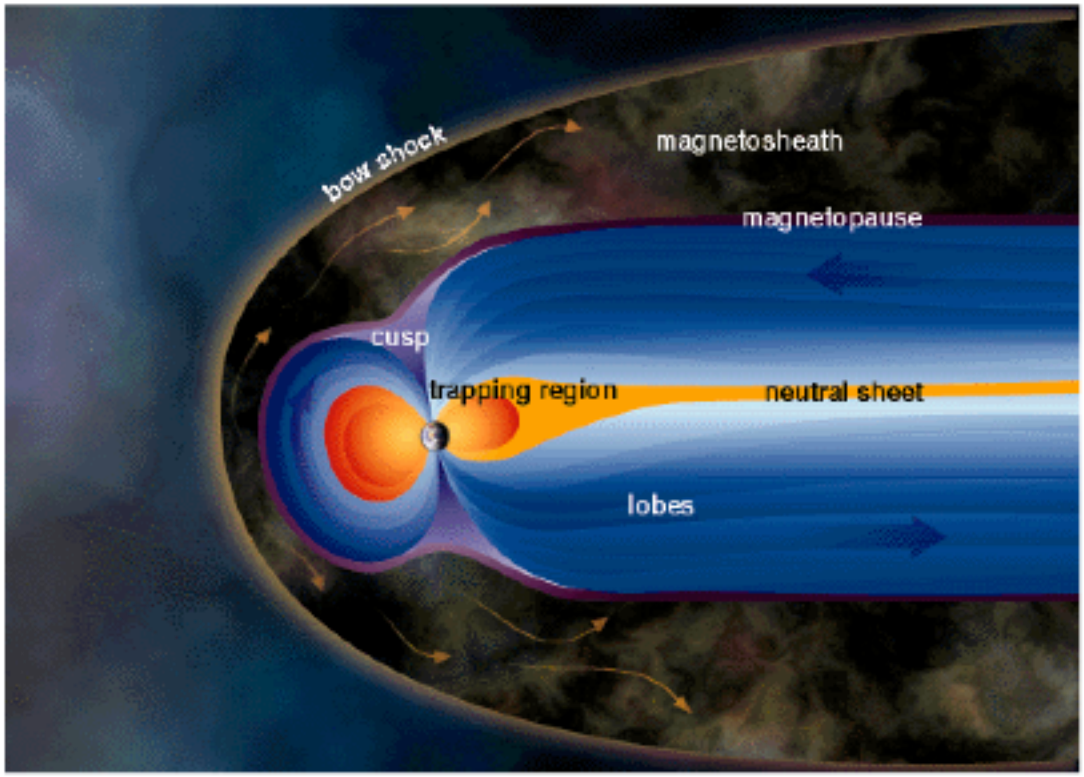

Drawing of Earth's magnetosphere. Notice that the magnetic field is much larger than the planet! *Windows Original Image*

Last modified prior to September, 2000 by the Windows Team

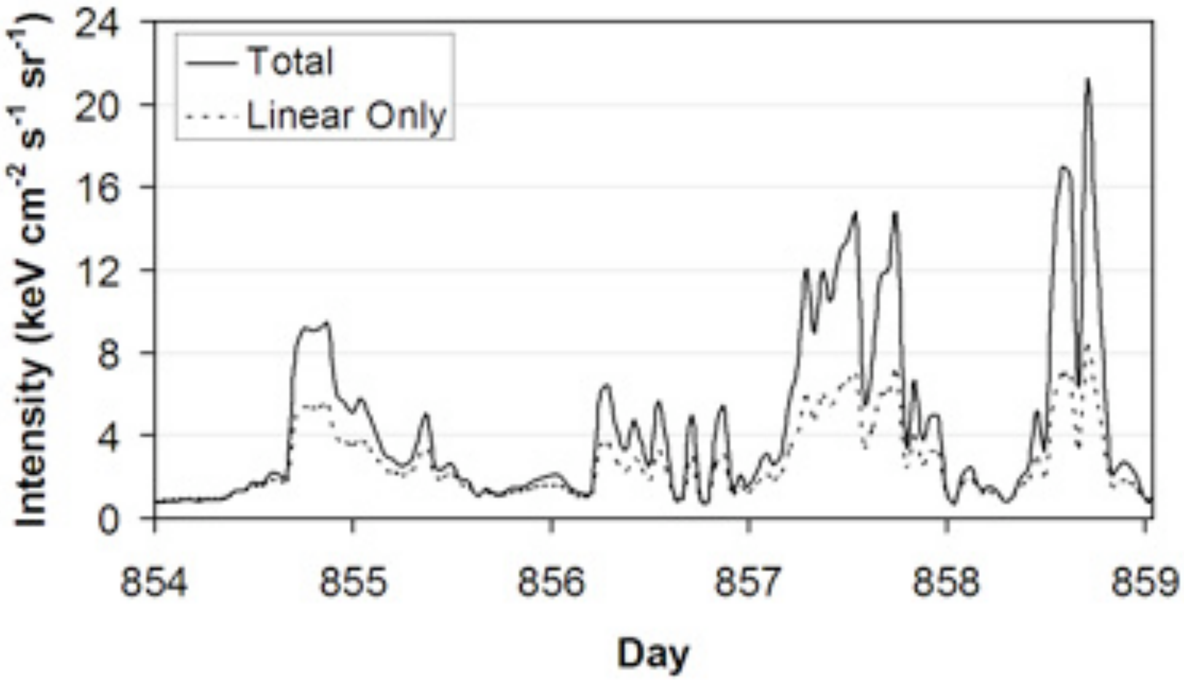

Robertson and Cravens

Wargelin et al. (2004)
CXO X-Ray Spectrum of Dark Side of Moon
(geocoronal x-rays) -- looks like SWCX x-rays.

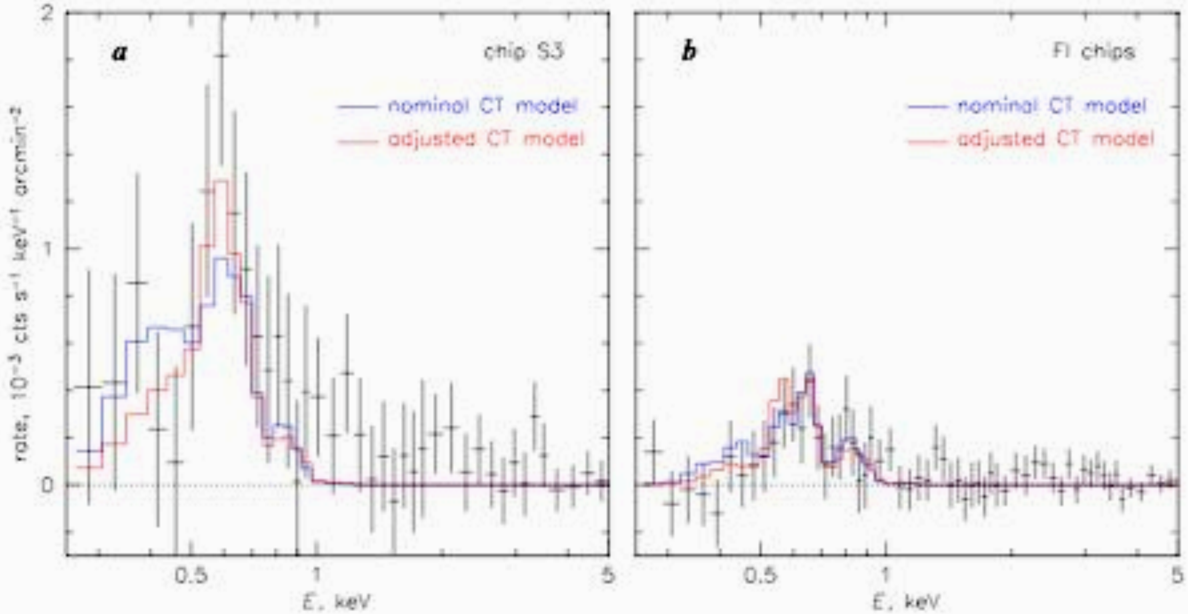

Fig. 6.— Background-subtracted September spectra (3 brightest ObsIDs) and charge transfer model fits using four composite lines. The same model, including normalization, is used to fit the S3 and FI spectra. The nominal fit uses the average (baseline) solar-wind parameters discussed in the text. In the adjusted fit, the relative C VI vs O VII Kα emission is 1/6 of the nominal case, and O VIII emission is reduced by half. Results for the adjusted fit are listed in Table 7.

Interaction of Interstellar Medium with Heliosphere

- Using the velocity vectors in the data (see image), we numerically calculated the solar wind streamlines. We then followed the evolution of solar wind ion ionization states along the stream lines and simultaneously determined the charge exchange production rates as a function of position.
- Using these 3D production rates, we produced 2D X-ray maps (photons/cm^2/s).

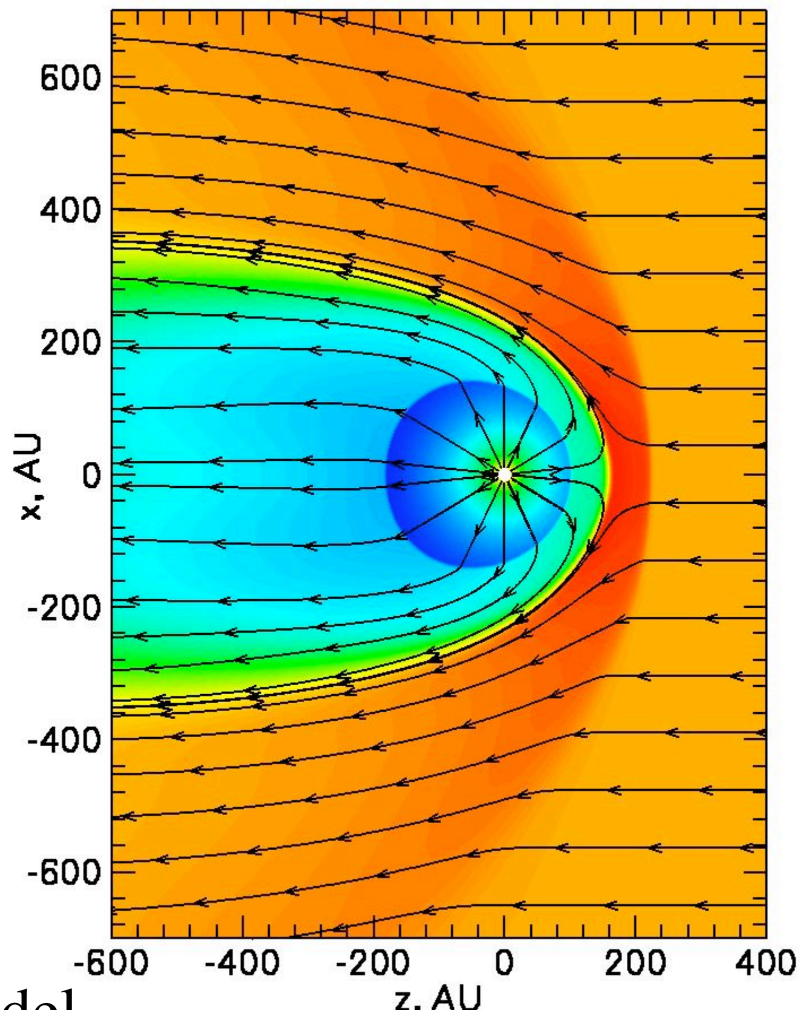

Zank and Florinski heliosphere model

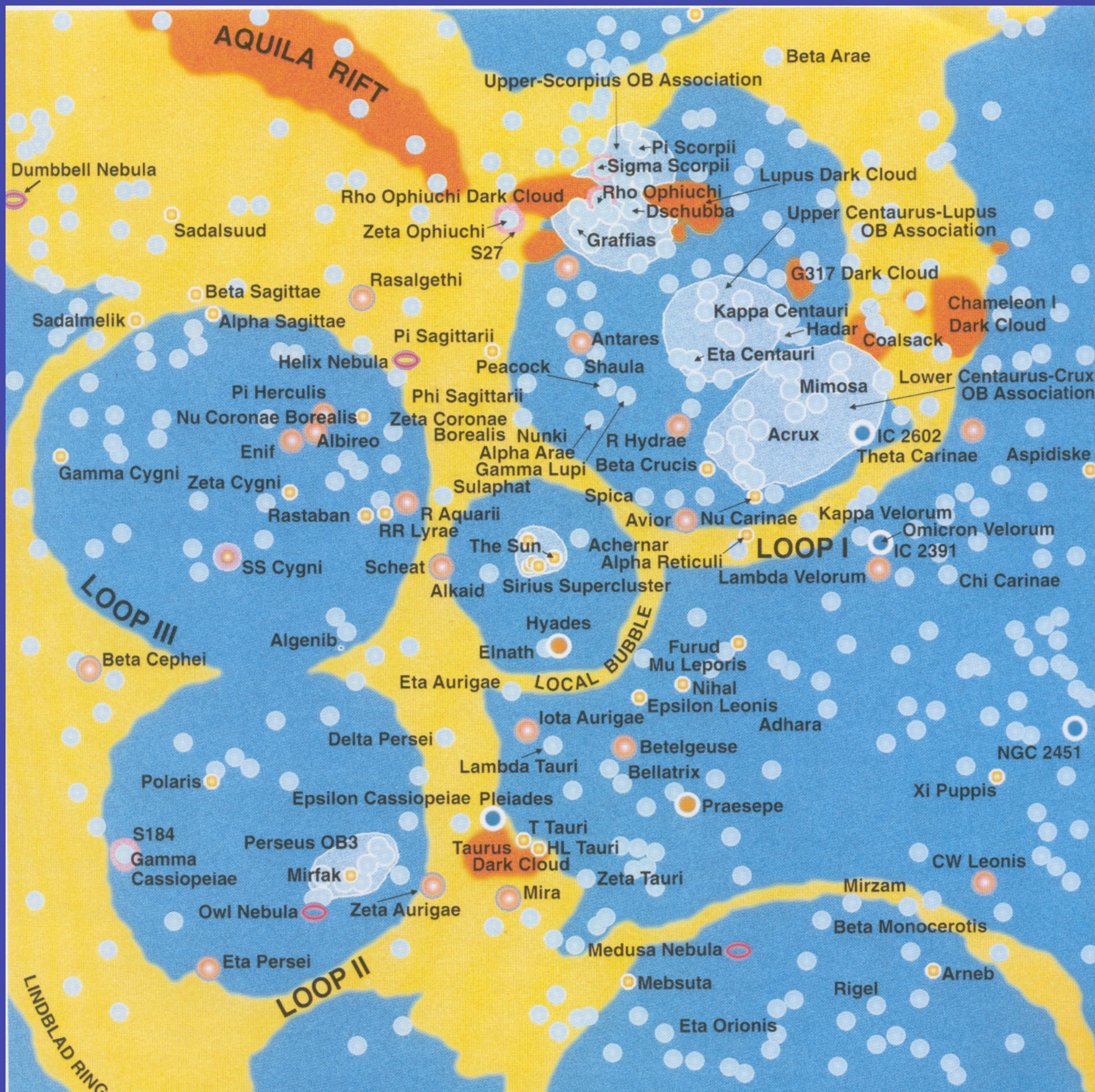

From Henbest and Cooper (1994).

500 pc by 500 pc view of galactic plane near the Sun.

Interstellar Medium

The Tail Beam Spectrum

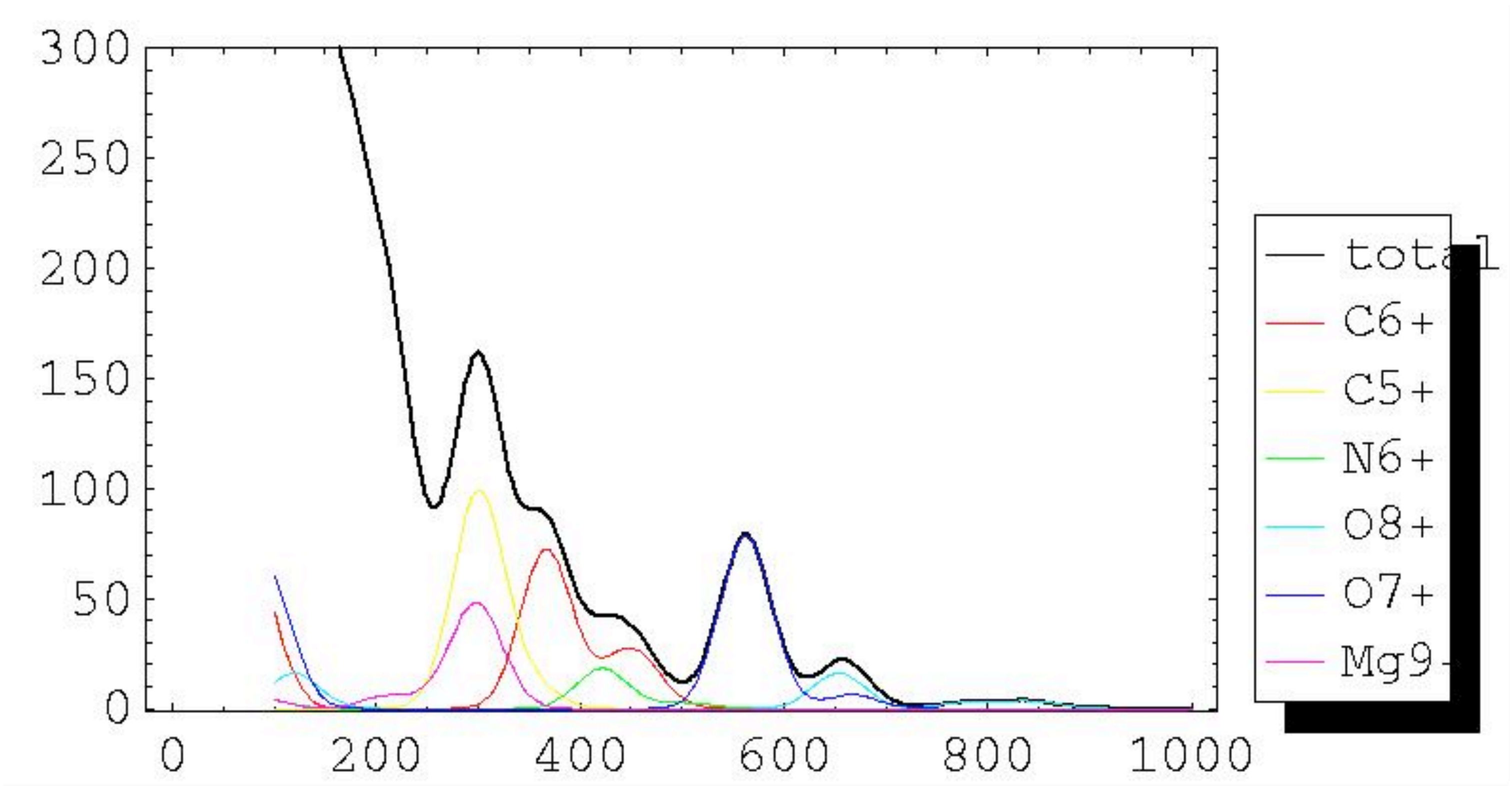

X-axis: photon energy
in units of eV

The Evolution of Ne^{8+}

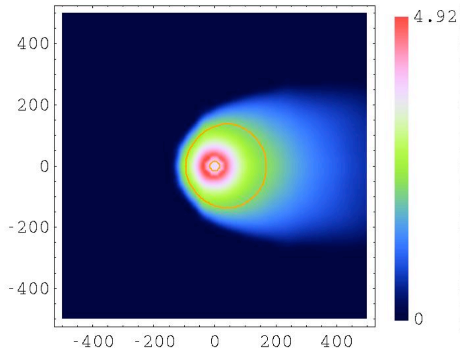

Ne^{8+}

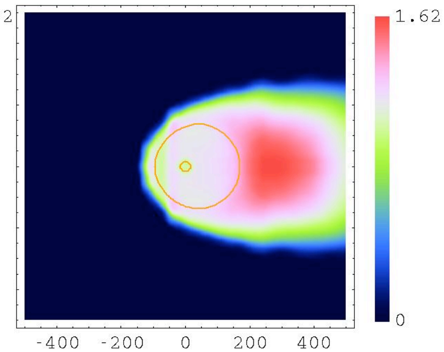

Ne^{7+}

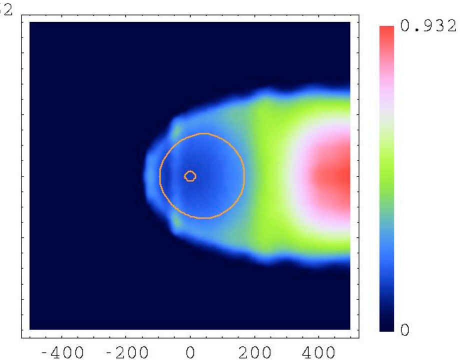

Ne^{6+}

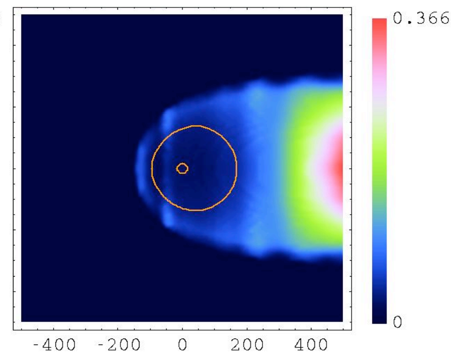

Ne^{5+}

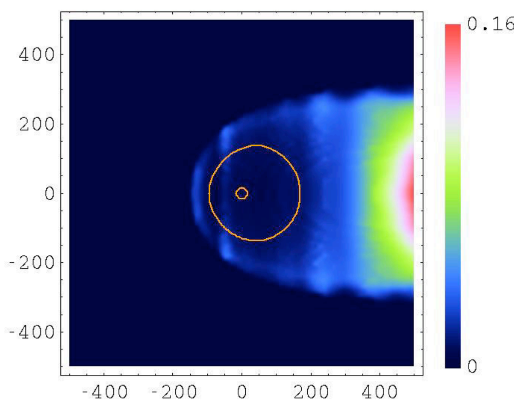

Ne^{4+}

The shown figures are modeled X-ray maps as observed from outside the heliosphere starting with Ne^{8+}. The maps show the transition of the original species to the emitting species. For instance, "Ne^{8+}" represents a map of the transition of $Ne^{8+} \rightarrow Ne^{7+}$,where Ne^{7+} emits the photon. The large orange contour represents the position of the termination shock, and the small one encircles the position of the Sun. Units are (photons/cm^2/s).

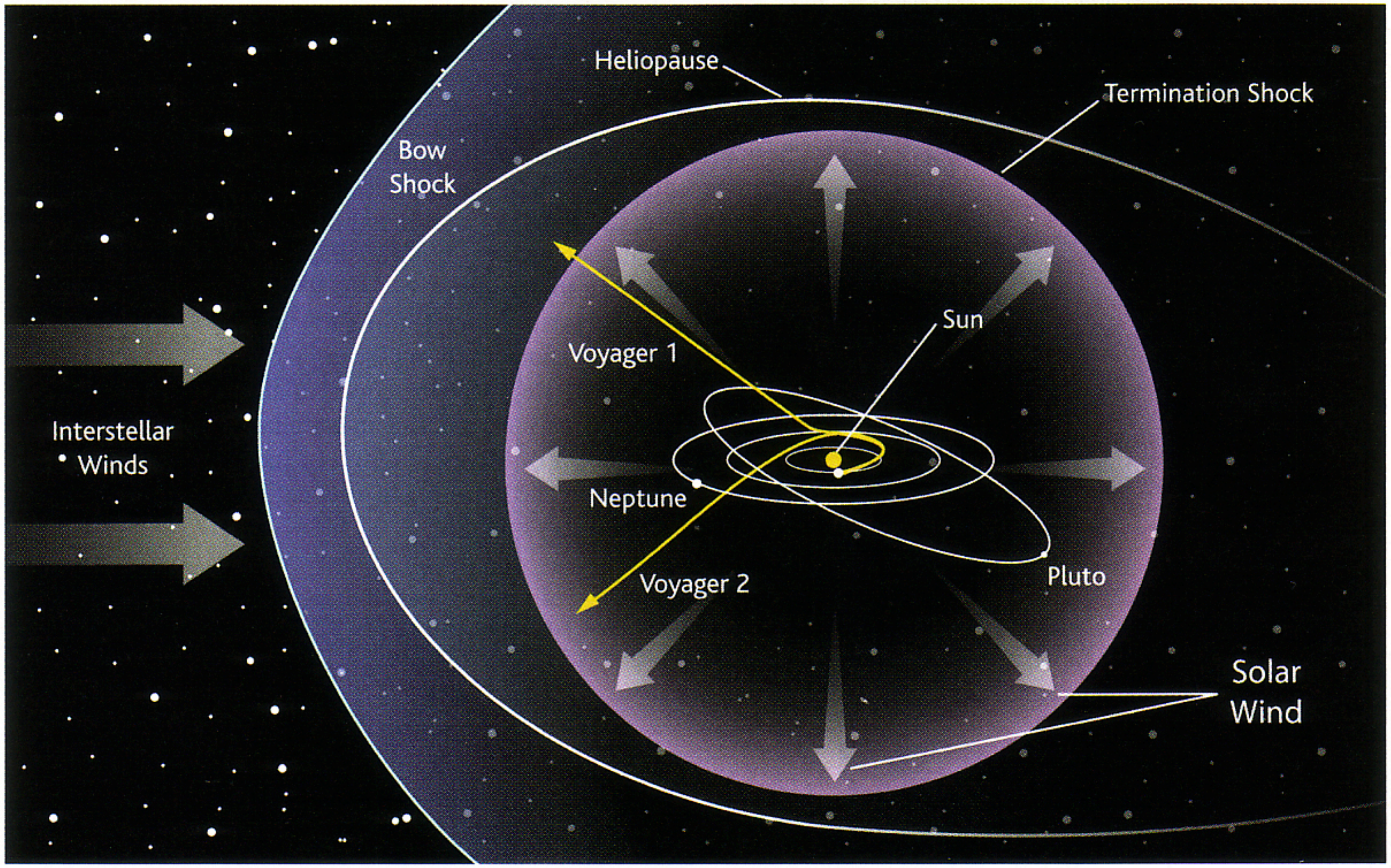

Fig. 1. Voyagers 1 and 2 have flown on different trajectories past the outer planets of the solar system since 1977, and Voyager 1 is reported to have crossed the termination shock of the solar wind at 94 AU from the Sun in December 2004. The solar wind is a supersonic flow, and a shock—the termination shock—is required for the wind to decelerate and merge with the local interstellar medium that bounds the solar system. The solar wind and interstellar gas do not merge easily, so further out beyond the termination shock, there is a true boundary between the solar wind and the interstellar medium: the heliopause. Further out still, if the solar system is itself moving supersonically relative to the interstellar medium, there may be a large bow shock.

Fisk (2005) -- Heliosphere Schematic

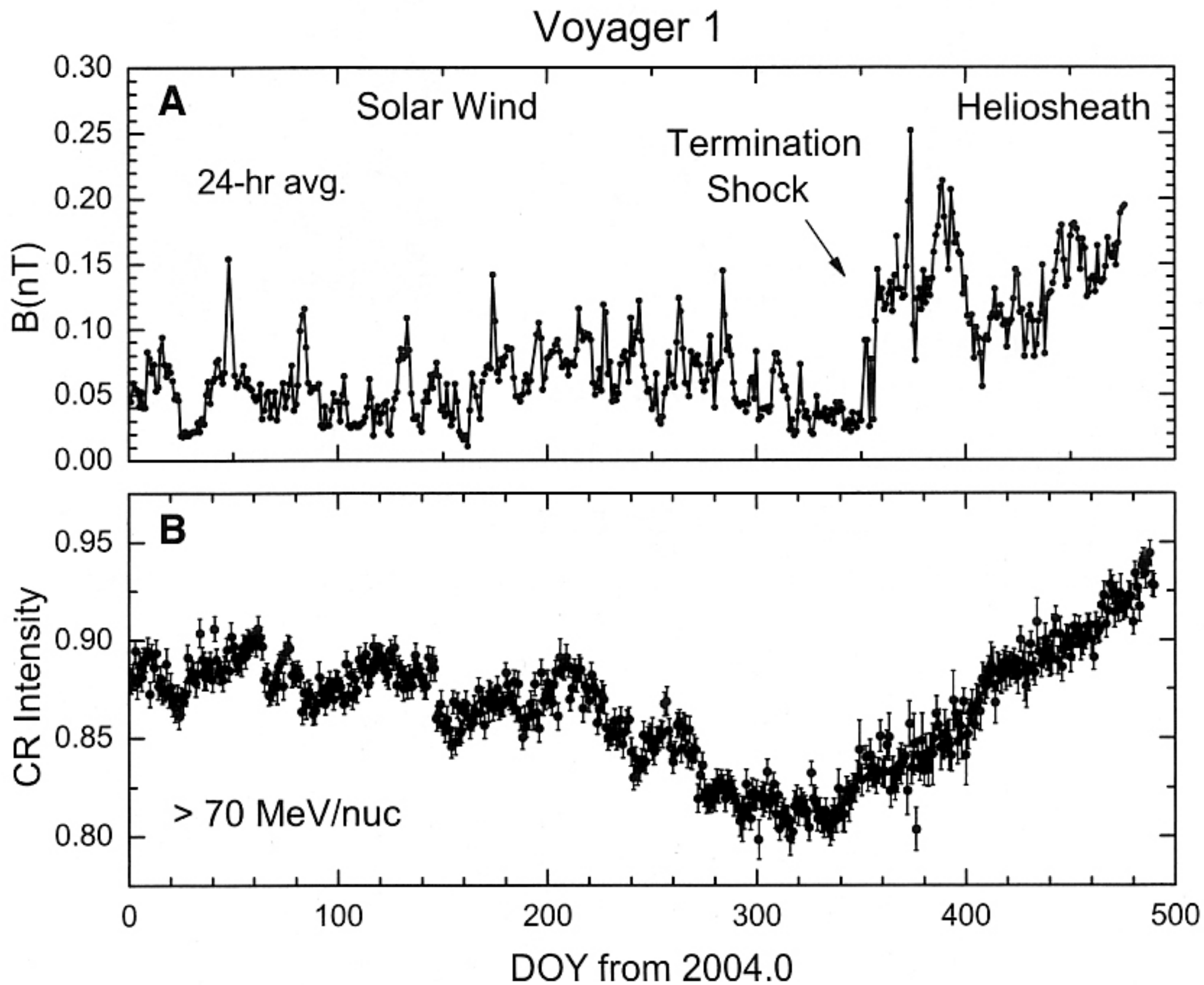

Fig. 4. The relationship between daily averages of the magnetic field strength (**A**) and the intensity of cosmic rays (CR) (**B**) in the heliosheath is different from that in the solar wind. Error bars show means ± SD. DOY, day of year.

Astronomy and Astrophysics, 2006:
Charge-TransferinducedEUVandSoftX-ray emissions inthe Heliosphere
D.Koutroumpa[1], R.Lallement[1], V.Kharchenko[2],A.Dalgarno[2],R.Pepino[2],V.Izmodenov[3],andE.Qu´ emerais[1]

X-RAY AND EXTREME ULTRAVIOLET EMISSIONS FROM COMETS VLADIMIR A. KRASNOPOLSKY1 , JASON B. GREENWOOD2 and PHILLIP C. STANCIL3

Space Science Reviews (2005)

Laboratory Simulation of Charge Exchange produced X-Ray Emission from Comets using the Spare *ASTRO-E* Microcalorimeter P. Beiersdorfer*, K. R. Boyce, G. V. Brown, H. Chen, S. M. Kahn , R. L. Kelley, M. May, R. E. Olson, F. S. Porter, C. K. Stahle , W. A. Tillotson

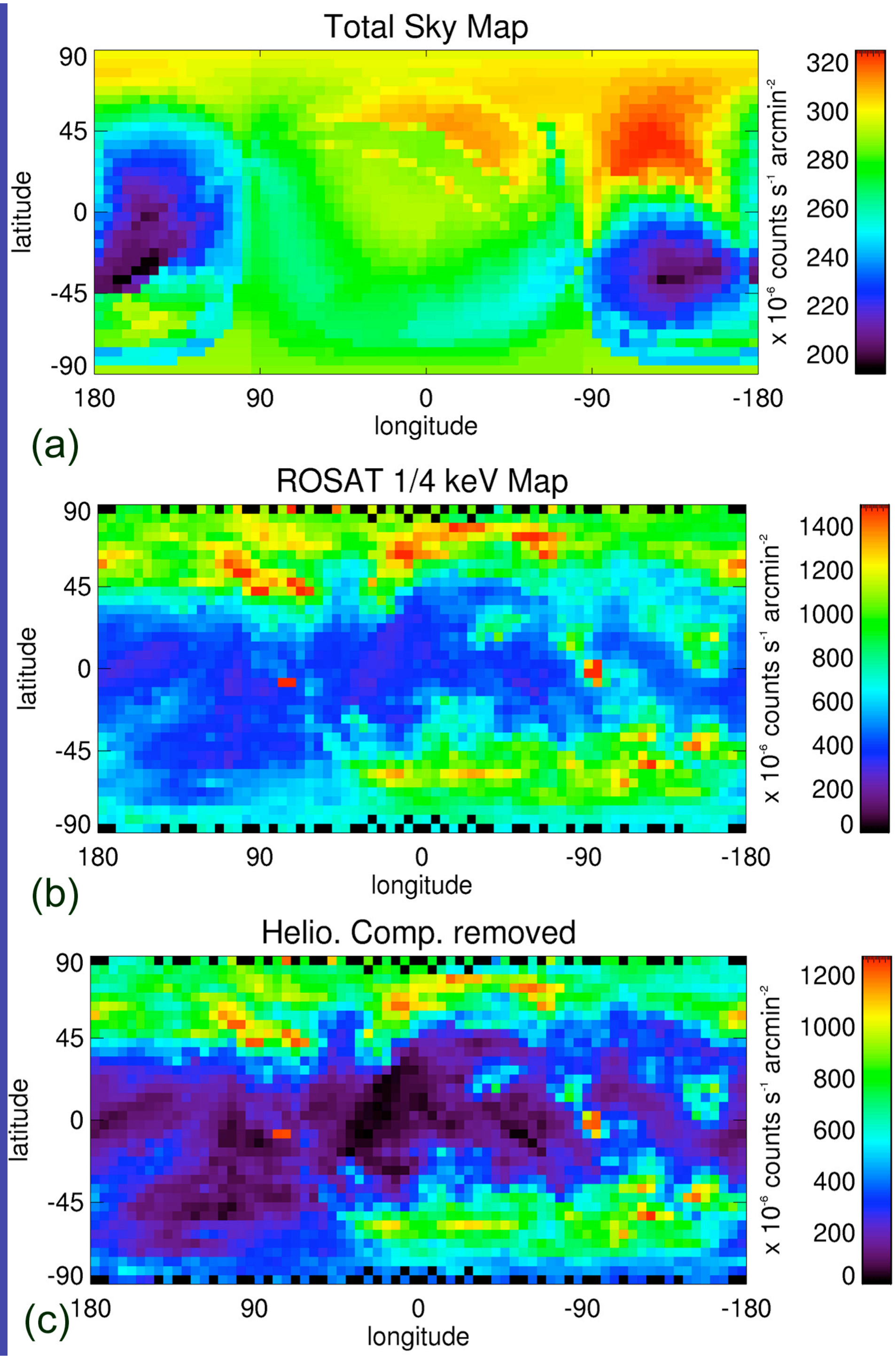

Predicted Heliospheric X-Ray Emission as seen From Earth.
-- in galactic coordinates.

Robertson, Cravens, and Snowden (2003).

ROSAT SXRB
Map is also shown and a *preliminary* "subtraction" map.